



## Material similarity of scaled models

Shuai Wang <sup>a,b</sup>, Fei Xu <sup>a,b,\*</sup>, Xiaoyu Zhang <sup>a,b</sup>, Leifeng Yang <sup>a,b</sup>, Xiaochuan Liu <sup>c</sup>

<sup>a</sup> School of Aeronautics, Northwestern Polytechnical University, Xi'an 710072, Shaanxi, China

<sup>b</sup> Institute for Computational Mechanics and Its Applications, Northwestern Polytechnical University, Xi'an 710072, Shaanxi, China

<sup>c</sup> Aviation Key Laboratory of Science and Technology on Structures Impact Dynamics, Aircraft Strength Research Institute of China, Xi'an 710065, China



### ARTICLE INFO

#### Keywords:

Material number  
Similarity  
Scaling  
Strain hardening  
Strain rate  
Thermal softening  
Structural impact

### ABSTRACT

When different strain hardening, strain-rate sensitive and temperature softening materials are used for scaled model and prototype, the traditional similarity laws of solid mechanics will be broken. Although research works in the last twenty years have developed the correction methods of initial conditions to compensate for the similarity distortion, their basic correction factors are practically impeded for their inherent non-direct (depending on unknown structural responses) and inexact (having significant similarity errors) defects. In this paper, a more complete framework of material similarity is developed. Based on the similarity analysis of thermo-visco-plastic constitutive equation, the material dimensionless numbers are suggested to represent the objective similarity of strain hardening, strain-rate sensitive and temperature softening effects. The universal direct and exact solution of the basic correction factors is further proved when the material numbers of the scaled model and the prototype are equal, which overcomes the previous inherent defects radically. And the simple and practical phase diagram of 'material numbers - strain/strain-rate/temperature' curves are proposed to design the optimum similitude materials. Three impacted structure are numerically verified: circular plate, crooked plate, and Taylor bar. The results show that the proposed material numbers control the similarity behavior of different materials. When the proposed direct and exact methods are used by the designed optimum similitude materials, the completely different materials can behave acceptable exact similarity of strain, strain-rate, temperature, stress and displacement responses in time and space fields.

### 1. Introduction

When the structural impact was studied by theoretical and numerical approaches, verification by experiment is indispensable. As an important approach, the use of a scaled model instead of the full-size prototype has a great practical advantage [1, 2]. The methodology relating the prototype (p) and the scaled model (m) is termed as similarity, scaling or similitude [3], and usually uses scaling factors of the physical quantities to conduct the forward scaling and the reverse prediction [1, 3]. For example, the basic geometric scaling factor is defined as  $\beta = \bar{L}_m / \bar{L}_p$  [3] to relate the structural characteristic lengths  $\bar{L}$ . For the physical quantity X, a general notation could be defined,  $\beta_X = (X)_m / (X)_p$ . In solid mechanics, scaling of the geometry, materials and external loads is the basic premise to establish similarity laws [3].

The traditional similarity laws were well-known and had been widely used in solid mechanics [3-6]. In this similarity system, the identical materials were considered to simplify similarity difficulties of

various material and constitutive parameters, and the pure geometrical scaling with single basic factor  $\beta$  was accomplished to relate various physical quantities between prototype and scaled model [3, 4]. However, the traditional similarity laws were easily broken for the non-scalabilities such as the size effects of material strain-rate sensitivity, gravity and fracture [3, 4, 7-11]. The non-scalability that violating the traditional similarity laws was usually called to be distorted [3].

The size effects of material strain-rate sensitivity were widespread [12], prompting researchers to develop the scaling method with correction factors in the last twenty years [13-18]. Oshiro and Alves [14] for example used a basic correction factor of impact velocity to compensate for distortion of material strain-rate effects. For simple analytical models [14] and even complex numerical models [15] with the strain-rate sensitive mild steel, this method only had relatively small prediction errors for overall responses. Similarly, the basic correction factor of mass/density for the impactor and structure were also developed in early work [16] and in recent works [17, 18]. However, these

\* Corresponding author: Dr. Fei Xu, Northwestern Polytechnical University, School of Aeronautics, P.O. Box 184, Xi'an, Shaanxi 710072, China  
E-mail address: [xufei@nwpu.edu.cn](mailto:xufei@nwpu.edu.cn) (F. Xu).

**Table 1**

Main scaling relationships of impact mechanics in geometrically-similar scaling.

Variable	Scaling factor	Variable	Scaling factor
Length, $\bar{L}$	$\beta = \bar{L}_m/\bar{L}_p$	Strain-rate, $\dot{\epsilon}$	$\beta_{\dot{\epsilon}} = \beta_V/\beta$
Density, $\rho$	$\beta_{\rho} = \rho_m/\rho_p$	Time, $t$	$\beta_t = \beta/\beta_V$
Velocity, $V$	$\beta_V = V_m/V_p$	Displacement, $\delta$	$\beta_{\delta} = \beta$
Temperature, $T$	$\beta_T = T_m/T_p$	Mass, $\bar{m}$	$\beta_{\bar{m}} = \beta_{\rho}\beta^3$
Stress, $\sigma$	$\beta_{\sigma} = \beta_{\rho}\beta_V^2$	Specific heat, $\alpha$	$\beta_{\alpha} = \beta_V^2/\beta_T$
Strain, $\epsilon$	$\beta_{\epsilon} = 1$	Energy, $E$	$\beta_E = \beta_{\rho}\beta^3\beta_V^2$

developed methods were limited by an inherent non-direct defect that the basic correction factors cannot be calculated directly due to their solvers depending on the unknown structural dynamic strain-rate responses [19]. Although the defect was alleviated by using the average strain-rate approximately instead of the unknown dynamic responses, it was very difficult to obtain the average value for most real structures [19]. To overcome this difficulty, a special power law constitutive equation was used to obtain a direct correction factor that has nothing to do with the structural dynamic response in the work of Oshiro and Alves [19]. When using simple analytical models, this direct correction factor produced perfect exact similarity. Nevertheless, it was only applicable to the particular power law form of the constitutive equation, not in all types.

Previous studies have assumed that a completely identical material was used for scaled model and prototype, and in fact, few experiments can satisfy this premise condition due to the absence of identical materials and the change of material properties in manufacturing [20]. In addition, impact problems usually involved many thermo-visco-plastic (i.e., strain hardening, strain-rate and temperature effects) constitutive parameters, so the use of different materials at scaling was an open complicated problem. Based on the previous average strain-rate method of correction factor, Alves and Oshiro [20] compensated for the similarity distortion of different materials that only considering the differences in quasi-static flow stress and strain-rate sensitive effects. Although this method was precise for simple analytical models [20], it had been verified to have significant errors for a more complex case of circular tubes axially impact experiment [21]. Mazzariol, et al. [22, 23] used the basic correction factor of impact mass / density to compensate for the similarity distortion of different materials that further considering the differences in density. In this work, the unknown strain-rate was approximately set to  $1 s^{-1}$  to simplify the previous non-direct defect in the solution of basic correction factor. Some different materials behaved good similarity, while others had very significant errors, especially for the strain-rate responses [22]. A more comprehensive consideration for the similarity distortion of different materials that further considering the differences in strain-hardening effects, temperature softening effects and failure are developed by Sadeghi et al. [24, 25]. In the work, instead of using unknown values of strain, strain-rate, and temperature, which depend on the structure response, a new technique adopted average values to represent a defined range of these variables. However, this technique usually resulted in obvious similarity errors and therefore was inexact. In the latest research, Wang and Xu et al. [26, 27] proposed geometric distortion similarity ability through adding a basic correction factor of geometrical thickness to compensate for distortion of the different materials. But the basic correction factors still depended on the previous method of the average strain and strain-rate.

Although the correction factor methods had been proved successful in compensating for the material similarity distortion, for most real structures, the previous studies were usually limited by the non-direct defect. In addition, as found in the research of our concerns, none of these previous studies were precise enough in predicting prototype responses, and therefore, they also had the inexact defect. The non-direct and inexact defects had impelled some researchers to examine the

influence of material selection for the similarity. By using virtual similitude materials, Sadeghi et al. [24, 25] obtained exact similarity results for complex numerical models. However, this technique cannot be used for the scaled experiment due to the unpractical difficulty of finding a material in which all parameters are specific. Wang and Xu et al. [28] qualitatively studied the influence of the material parameters for the optimal similarity of dynamic flow stress and found that the strain-rate sensitivity parameters played a more decisive role. Davey et al. [29] qualitatively studied influence of the Hansel-Spittel constitutive parameters for similarity and obtained more exact scaling feasibility for the complicated hot forging experimentation. In spite of this, these studies only focused on qualitative discussions for specific material parameters in particular constitutive models. For the previous non-direct and inexact defects, nor did they offer fundamental and universal solutions. This fact forms the basic motivation for our study reported here. In this paper, a more complete framework of material similarity, based on the new proposed material dimensionless numbers of strain hardening, strain-rate sensitive and temperature softening effects, is suggested to overcome the above two inherent defects. The framework allows not only the direct and exact calculation of the basic correction factor but also the quantitative analysis for the similarity of the different materials. More importantly, the material similarity is redefined by the proposed material dimensionless numbers, and therefore, more systematical research is developed on the basis of previous works.

In what follows, [Section 2](#) introduces our proposed material similarity framework in detail. [Section 3](#) respectively investigated three impacted numerical models with material strain hardening, strain-rate sensitive and temperature softening effects. [Section 4](#) summarizes this work.

## 2. Material similarity framework

### 2.1. A brief review of previous scaling approach

To overcome the similarity distortion of the different materials containing the strain hardening, strain-rate sensitive and temperature softening effects, recent researchers [13-28] have developed several new similarity systems to extend the scaling ability. Although their approaches used to establish similarity laws (such as dimensional analysis [14, 22, 26, 27] or equation analysis [24, 25]) could be different, the resulting scaling relationships are usually identical. In geometrically-similar scaling, main scaling relationships [24-27] are listed in [Table 1](#), in which  $\beta$ ,  $\beta_V$ ,  $\beta_{\rho}$  and  $\beta_T$  are four independent basic scaling factors. Then, the forward scaling and the reverse prediction from prototype to scaled model can be conduct by these relationships.

Different from the traditional similarity laws, which assumes  $\beta_{\rho} = 1$ ,  $\beta_V = 1$  and  $\beta_T = 1$  [3, 4] in [Table 1](#) and uses identical materials, the new developed systems usually compensate for the similarity distortion of the different materials by correcting the initial velocity, density, geometry and temperature conditions of scaled model. Since these correction methods can convert to each other [24-27], the velocity correction and geometrically-similar scaling, as one of the typical representatives, is mainly discussed in the present paper. The velocity correction factor is defined as follows.

Consider the thermo-visco-plastic constitutive equation including strain hardening, strain-rate sensitive and temperature softening effects,

$$\sigma_d = \sigma_0 f(\epsilon, \dot{\epsilon}, T), \quad (1)$$

where  $\sigma_0$  and  $\sigma_d$  are the quasi-static and dynamic flow stress, respectively;  $f$  is function.

The similarity theory requires the consistency between the predicted stress,  $(\sigma_d)_m/\beta_{\sigma}$ , by scaled model and the stress of prototype,  $(\sigma_d)_p$ , i.e.  $(\sigma_0)_m f_m(\epsilon_m, \dot{\epsilon}_m, T_m)/\beta_{\sigma} = (\sigma_0)_p f_p(\epsilon_p, \dot{\epsilon}_p, T_p)$  [24, 25, 27]. When combining the scaling relations  $\beta_{\sigma} = \beta_{\rho}\beta_V^2$ ,  $\beta_{\epsilon} = 1$ ,  $\beta_{\dot{\epsilon}} = \beta_V/\beta$  and  $\beta_T =$

$T_m/T_p$ , the consistency equality of stress can derive the correction factor of velocity [14, 22, 24-27] as

$$\beta_V = \sqrt{\frac{\beta_{\sigma_d}}{\beta_\rho}} = \sqrt{\frac{\beta_{\sigma_0} f_m(\beta_e \epsilon_p, \beta_{\dot{e}} \dot{\epsilon}_p, \beta_T T_p)}{\beta_\rho f_p(\epsilon_p, \dot{\epsilon}_p, T_p)}} = \sqrt{\frac{\beta_{\sigma_0} f_m(\epsilon_p, (\beta_V/\beta) \dot{\epsilon}_p, \beta_T T_p)}{\beta_\rho f_p(\epsilon_p, \dot{\epsilon}_p, T_p)}},$$

$$(or, \beta_V = \sqrt{\frac{\beta_{\sigma_0} f_m(\epsilon_m, \dot{\epsilon}_m, T_m)}{\beta_\rho f_p(\epsilon_m / \beta_e, \dot{\epsilon}_m / \beta_{\dot{e}}, T_m / \beta_T)}} = \sqrt{\frac{\beta_{\sigma_0} f_m(\epsilon_m, \dot{\epsilon}_m, T_m)}{\beta_\rho f_p(\epsilon_m, \dot{\epsilon}_m / (\beta_V/\beta), T_m / \beta_T)}}}$$

$$(2)$$

which can be solved by a numerical method if the structural responses of the strain  $\epsilon_p$ , the strain-rate  $\dot{\epsilon}_p$  and the temperature  $T_p$  (or  $\epsilon_m$ ,  $\dot{\epsilon}_m$  and  $T_m$ ) are known. It should be noted that  $\beta_T$  is defined by the relation  $\beta_a = \beta_V^2 / \beta_T$  [25].

In the above correction procedure, understanding Eq. (2) is crucial since it was usually regarded as a very key technique to overcome the traditional similarity law defects. However, as mentioned in Section 1, two main inherent defects, existing in all previous developed approaches, can be found as follows.

- Non-direct defect: the correction factor  $\beta_V$  in Eq. (2) cannot be solved directly since it depends on the unknown structural dynamic responses of  $(\epsilon_p, \dot{\epsilon}_p, T_p)$  or  $(\epsilon_m, \dot{\epsilon}_m, T_m)$ . So far, a direct solution  $\beta_V = \rho^{n_2/(n_2-2)}$  [19] without the structural responses is founded only for the identical materials with the power law equation  $\sigma_d = \sigma_0(\dot{\epsilon}/\dot{\epsilon}_0)^{n_2}$  (the physical meanings of  $\dot{\epsilon}_0$  and  $n_2$  can be seen in Eq. (15)). However, there is no universal direct solution for scaling of different materials and any constitutive equation [28].
- Inexact defect: the substitution of different structural dynamic responses into Eq. (2) will lead to different values of  $\beta_V$ , while the similarity theory requires only one value of  $\beta_V$ , which means the consistency equality  $(\sigma_0)_m f_m(\epsilon_m, \dot{\epsilon}_m, T_m) / \beta_\sigma = (\sigma_0)_p f_p(\epsilon_p, \dot{\epsilon}_p, T_p)$  cannot always be precisely satisfied for dynamic impact process. As a result, the previous research works, which use the average values [14-16, 18, 20, 21, 26, 27], some particular values [17, 22, 23] and fixed window [24, 25, 28] of  $\epsilon_p$ ,  $\dot{\epsilon}_p$  and  $T_p$  to obtain an approximation of  $\beta_V$ , always behave even very significant similarity errors. A more intuitive and forceful explanation of the inexactness influence is given in Appendix A.

Therefore, it is imperative to expand the previous methodologies by further overcoming the non-direct and inexact defects.

## 2.2. Dimensionless numbers of material similarity

To derive the essential similarity criterion for strain hardening, strain-rate sensitive and temperature softening materials, in what follows, we further investigate similarity of the material second-order effects by the slope of the most basic stress - strain/strain-rate/temperature relation.

Without loss of generality, the total differential relation (or one-dimensional incremental relation of plasticity) of the constitutive equation Eq. (1) is expressed as

$$\begin{aligned} d\sigma_d &= \sigma_0 \frac{\partial f(\epsilon, \dot{\epsilon}, T)}{\partial \epsilon} d\epsilon + \sigma_0 \frac{\partial f(\epsilon, \dot{\epsilon}, T)}{\partial \dot{\epsilon}} d\dot{\epsilon} + \sigma_0 \frac{\partial f(\epsilon, \dot{\epsilon}, T)}{\partial T} dT \\ &= E_t(\epsilon, \dot{\epsilon}, T) d\epsilon + K_t(\epsilon, \dot{\epsilon}, T) d\dot{\epsilon} + R_t(\epsilon, \dot{\epsilon}, T) dT, \end{aligned} \quad (3)$$

where  $E_t(\epsilon, \dot{\epsilon}, T) = \sigma_0 \partial f(\epsilon, \dot{\epsilon}, T) / \partial \epsilon$ ,  $K_t(\epsilon, \dot{\epsilon}, T) = \sigma_0 \partial f(\epsilon, \dot{\epsilon}, T) / \partial \dot{\epsilon}$  and  $R_t(\epsilon, \dot{\epsilon}, T) = \sigma_0 \partial f(\epsilon, \dot{\epsilon}, T) / \partial T$  are material tangent modulus. Apparently, besides the dynamic flow stress  $\sigma_d$ , the important material parameters  $E_t$ ,  $K_t$  and  $R_t$  appear.

For two different materials with similarity, Eq. (3) can be written as

$$d(\sigma_d)_m = (E_t)_m d\epsilon_m + (K_t)_m d\dot{\epsilon}_m + (R_t)_m dT_m \quad (4a)$$

and

$$d(\sigma_d)_p = (E_t)_p d\epsilon_p + (K_t)_p d\dot{\epsilon}_p + (R_t)_p dT_p, \quad (4b)$$

respectively.

The substitution of  $(\sigma_d)_m = \beta_{\sigma_d}(\sigma_d)_p$ ,  $(E_t)_m = \beta_{E_t}(E_t)_p$ ,  $(K_t)_m = \beta_{K_t}(K_t)_p$ ,  $(R_t)_m = \beta_{R_t}(R_t)_p$ ,  $\epsilon_m = \beta_e \epsilon_p$ ,  $\dot{\epsilon}_m = \beta_{\dot{e}} \dot{\epsilon}_p$  and  $T_m = \beta_T T_p$  into Eq. (4a) leads to

$$d(\beta_{\sigma_d}(\sigma_d)_p) = \beta_{E_t}(E_t)_p d(\beta_e \epsilon_p) + \beta_{K_t}(K_t)_p d(\beta_{\dot{e}} \dot{\epsilon}_p) + \beta_{R_t}(R_t)_p d(\beta_T T_p). \quad (5a)$$

It can be further rewritten as

$$d(\sigma_d)_p = \frac{\beta_{E_t} \beta_e}{\beta_{\sigma_d}} (E_t)_p d\epsilon_p + \frac{\beta_{K_t} \beta_{\dot{e}}}{\beta_{\sigma_d}} (K_t)_p d\dot{\epsilon}_p + \frac{\beta_{R_t} \beta_T}{\beta_{\sigma_d}} (R_t)_p dT_p. \quad (5b)$$

For similarity, Eq. (5b) and Eq. (4b) should be identical, which respects the quantitative similarity criterions

$$\frac{\beta_{E_t} \beta_e}{\beta_{\sigma_d}} = 1, \quad \frac{\beta_{K_t} \beta_{\dot{e}}}{\beta_{\sigma_d}} = 1 \quad \text{and} \quad \frac{\beta_{R_t} \beta_T}{\beta_{\sigma_d}} = 1. \quad (6a-c)$$

The three criterions can also be re-written as the three dimensionless equations

$$(\Pi_{E_t})_m = (\Pi_{E_t})_p, \quad (\Pi_{K_t})_m = (\Pi_{K_t})_p \quad \text{and} \quad (\Pi_{R_t})_m = (\Pi_{R_t})_p, \quad (7a-c)$$

respectively, where  $\Pi_{E_t} = \left[ \frac{E_t \epsilon}{\sigma_d} \right]$ ,  $\Pi_{K_t} = \left[ \frac{K_t \dot{\epsilon}}{\sigma_d} \right]$  and  $\Pi_{R_t} = \left[ \frac{R_t T}{\sigma_d} \right]$  are dimensionless numbers of the material strain hardening, strain-rate sensitive and temperature softening effects, respectively. It should be noted that Eqs. (7a)-(7c) establish the necessary conditions of similarity. For the full similarity of the impact problems, other conditions such as similarity of geometry and impact loads also need to be satisfied [3]. For example, according to Table 1, the impact mass G needs to satisfy the scaling factor  $\beta_G = \beta_p \beta^3$ . As it is not the subject of this article, more detailed discussion can be referred to Refs. [26]-[27].

It is easy to see that the numbers  $\Pi_{E_t}$ ,  $\Pi_{K_t}$  and  $\Pi_{R_t}$  are the dominant dimensionless parameters for material similarity. For convenience, the three dimensionless numbers are termed as "material similarity number / material number (Mn)" by the present paper and are further expressed as<sup>1</sup>

$$Mn\{\epsilon\} = \frac{E_t(\epsilon, \dot{\epsilon}, T)\epsilon}{\sigma_d} = \frac{(\partial f(\epsilon, \dot{\epsilon}, T)/\partial \epsilon)\epsilon}{f(\epsilon, \dot{\epsilon}, T)} = \frac{\partial \ln f(\epsilon, \dot{\epsilon}, T)}{\partial \ln \epsilon}, \quad (8a)$$

$$Mn\{\dot{\epsilon}\} = \frac{K_t(\epsilon, \dot{\epsilon}, T)\dot{\epsilon}}{\sigma_d} = \frac{(\partial f(\epsilon, \dot{\epsilon}, T)/\partial \dot{\epsilon})\dot{\epsilon}}{f(\epsilon, \dot{\epsilon}, T)} = \frac{\partial \ln f(\epsilon, \dot{\epsilon}, T)}{\partial \ln \dot{\epsilon}} \quad (8b)$$

and

$$Mn\{T\} = \frac{R_t(\epsilon, \dot{\epsilon}, T)T}{\sigma_d} = \frac{(\partial f(\epsilon, \dot{\epsilon}, T)/\partial T)T}{f(\epsilon, \dot{\epsilon}, T)} = \frac{\partial \ln f(\epsilon, \dot{\epsilon}, T)}{\partial \ln T}, \quad (8c)$$

respectively, where the curly braces  $\{\epsilon\}$ ,  $\{\dot{\epsilon}\}$  and  $\{T\}$  represent associations with the material strain hardening, strain-rate sensitive and

<sup>1</sup> For the material number  $Mn\{\dot{\epsilon}\}$ , the similar forms  $\lambda = [\partial \sigma / \partial \ln \dot{\epsilon}]$ ,  $[\partial \tau / \partial \ln \dot{\epsilon}]$ ,  $[\partial \tau_{eff} / \partial \ln \dot{\epsilon}]$  and  $[\partial \ln \sigma_d / \partial \ln \dot{\epsilon}]$  [30, 31], termed as the strain-rate sensitivity coefficient (or exponent), were used for macroscopic dynamic plasticity and dislocation dynamic studies, where  $\tau$ ,  $\dot{\epsilon}$  and  $\tau_{eff}$  were shear stress, shear strain-rate and effective shear stress [30], respectively. It is noted that the first three forms of  $\lambda$  have the dimension [MPa]; while the last form is a dimensionless number and equivalent to  $Mn\{\dot{\epsilon}\}$ .

temperature softening effects, respectively.

More generally, for similarity of arbitrary material effects, the material number  $Mn$  can be defined as the form

$$Mn\{X_i\} = \frac{[\partial f(X_1, \dots, X_i, \dots, X_N)/\partial X_i]X_i}{f(X_1, \dots, X_i, \dots, X_N)} = \frac{\partial \ln f(X_1, \dots, X_i, \dots, X_N)}{\partial \ln X_i} \quad (9)$$

for the general constitutive model  $\sigma = f(X_1, \dots, X_i, \dots, X_N)$  with  $N$  mechanical variables. The form  $\partial \ln(\text{function})/\partial \ln(\text{independent variable})$  is an important operator with dimensionless property. For example, for the linear elastic constitutive model  $\sigma = E^e \varepsilon^e$ , the material number is defined as  $Mn\{\varepsilon^e\} = \partial \ln \sigma / \partial \ln \varepsilon^e \equiv 1$ , where  $E^e$  and  $\varepsilon^e$  are Young's modulus and elastic strain, respectively. It is easy to prove that if the maximum linear elastic strain  $\varepsilon_{max}^e$  satisfy  $(\varepsilon_{max}^e)_m / (\varepsilon_{max}^e)_p = \beta_e$  (i.e.,  $(\sigma_0/E^e)_m / (\sigma_0/E^e)_p = \beta_e$ ), the elastic effects of all materials are always similar when Eq. (6a-c) is true in structural impact.

From Eq. (8a-c) follows that the material numbers can be considered as the ratio of a material's ability to maintain present flow stress (i.e.,  $E_t \varepsilon$  at space,  $K_t \dot{\varepsilon}$  at time and  $R_t T$  at temperature) to its own resistance (i.e.,  $\sigma_d$ ); they can also be considered as the rate of change of the logarithmic exponent of dynamic flow stress (i.e.,  $n = \ln f(\varepsilon, \dot{\varepsilon}, T)$  with  $n$  being exponent of the natural constant  $e$ ) relative to the logarithmic exponent of strain/strain-rate/temperature (i.e.,  $\ln \varepsilon$ ,  $\ln \dot{\varepsilon}$  and  $\ln T$ ); they can be also understood as the intrinsic requirement of similarity to material basic mechanical properties.

### 2.3. Direct and exact solution of correction factor

In an attempt to solve the inherent non-direct and inexact defects of previous approach, the material similarity criterion developed in Section 2.2 is applied.

The similarity criterion  $Mn_m\{\varepsilon_m\} = Mn_p\{\varepsilon_p\}$  (Eq. (7a)) leads to

$$\begin{aligned} \left\{ \frac{\partial \ln f_m(\varepsilon_m, \dot{\varepsilon}_m, T_m)}{\partial \ln \varepsilon_m} \right\} &= \frac{\partial \ln f_m(\beta_e \varepsilon_p, \beta_e \dot{\varepsilon}_p, \beta_T T_p)}{\partial \ln(\beta_e \varepsilon_p)} = \frac{\partial \ln f_m(\beta_e \varepsilon_p, \beta_e \dot{\varepsilon}_p, \beta_T T_p)}{\partial \ln \varepsilon_p} \\ &= \left\{ \frac{\partial \ln f_p(\varepsilon_p, \dot{\varepsilon}_p, T_p)}{\partial \ln \varepsilon_p} \right\} \rightarrow \frac{\partial \ln f_m(\beta_e \varepsilon_p, \beta_e \dot{\varepsilon}_p, \beta_T T_p)}{\partial \ln \varepsilon_p} = \frac{\partial \ln f_p(\varepsilon_p, \dot{\varepsilon}_p, T_p)}{\partial \ln \varepsilon_p} \end{aligned} \quad (10)$$

In order to integrate Eq. (10),  $\dot{\varepsilon}_p$  and  $T_p$  are assumed to be some arbitrary constant  $\dot{\varepsilon}_C$  and  $T_C$ , respectively. Then, Eq. (10) becomes the derivative relation

$$\partial \ln f_m(\beta_e \varepsilon_p, \beta_e \dot{\varepsilon}_C, \beta_T T_C) = \partial \ln f_p(\varepsilon_p, \dot{\varepsilon}_C, T_C) \quad (11)$$

So, the integral for Eq. (11) results in

$$\frac{f_m(\beta_e \varepsilon_p, \beta_e \dot{\varepsilon}_C, \beta_T T_C)}{f_p(\varepsilon_p, \dot{\varepsilon}_C, T_C)} = \text{constant} \quad (12a)$$

In a similar way, the similarity criterions  $Mn_m\{\dot{\varepsilon}_m\} = Mn_p\{\dot{\varepsilon}_p\}$  (Eq. (7b)) and  $Mn_m\{T_m\} = Mn_p\{T_p\}$  (Eq. (7c)) leads to

$$\frac{f_m(\beta_e \varepsilon_p, \beta_e \dot{\varepsilon}_p, \beta_T T_C)}{f_p(\varepsilon_p, \dot{\varepsilon}_p, T_C)} = \text{constant} \quad \text{and} \quad \frac{f_m(\beta_e \varepsilon_p, \beta_e \dot{\varepsilon}_p, \beta_T T_p)}{f_p(\varepsilon_p, \dot{\varepsilon}_p, T_p)} = \text{constant} \quad (12b-c)$$

respectively, where  $\varepsilon_p$  is also some arbitrary constant.

Apparently, Eq. (12a)-(12c) implies that the four dimensional surfaces  $z_m = f_m(\beta_e \varepsilon_p, \beta_e \dot{\varepsilon}_p, \beta_T T_p)$  and  $z_p = f_p(\varepsilon_p, \dot{\varepsilon}_p, T_p)$  are proportional on any cross section (i.e.,  $\varepsilon_p = \varepsilon_C$ ;  $\dot{\varepsilon}_p = \dot{\varepsilon}_C$ ;  $T_p = T_C$ ) perpendicular to the  $\varepsilon_p$ ,

$\dot{\varepsilon}_p$  and  $T_p$  axes. So, every point on the two surfaces is proportional, which leads to

$$\frac{f_m(\beta_e \varepsilon_p, \beta_e \dot{\varepsilon}_p, \beta_T T_p)}{f_p(\varepsilon_p, \dot{\varepsilon}_p, T_p)} = \text{constant} \quad \text{if} \begin{cases} Mn_m\{\varepsilon_m\} = Mn_p\{\varepsilon_p\} \\ Mn_m\{\dot{\varepsilon}_m\} = Mn_p\{\dot{\varepsilon}_p\} \\ Mn_m\{T_m\} = Mn_p\{T_p\} \end{cases}. \quad (13)$$

This means that the unknown responses  $\varepsilon_p$ ,  $\dot{\varepsilon}_p$  and  $T_p$  can be canceled out from Eq. (13). To better represent this result, the arbitrary values of the strain, strain-rate and temperature,  $\hat{\varepsilon}_p$ ,  $\hat{\dot{\varepsilon}}_p$  and  $\hat{T}_p$ , that are independent of the structural responses, are used to instead of  $\varepsilon_p$ ,  $\dot{\varepsilon}_p$  and  $T_p$ , respectively. Then, the universal direct and exact solution for Eq. (2) can be obtained as

$$\begin{aligned} \beta_V &= \sqrt{\frac{\beta_{\sigma_0} f_m(\beta_e \hat{\varepsilon}_p, \beta_e \hat{\dot{\varepsilon}}_p, \beta_T \hat{T}_p)}{\beta_\rho f_p(\hat{\varepsilon}_p, \hat{\dot{\varepsilon}}_p, \hat{T}_p)}} \\ &= \sqrt{\frac{\beta_{\sigma_0} f_m(\hat{\varepsilon}_p, (\beta_V/\beta) \hat{\dot{\varepsilon}}_p, \beta_T \hat{T}_p)}{\beta_\rho f_p(\hat{\varepsilon}_p, \hat{\dot{\varepsilon}}_p, \hat{T}_p)}} = \text{constant} \quad \text{if} \begin{cases} Mn_m\{\varepsilon_m\} = Mn_p\{\varepsilon_p\} \\ Mn_m\{\dot{\varepsilon}_m\} = Mn_p\{\dot{\varepsilon}_p\} \\ Mn_m\{T_m\} = Mn_p\{T_p\} \end{cases} \end{aligned} \quad (14)$$

which makes the consistency equality  $(\sigma_0)_m f_m(\varepsilon_m, \dot{\varepsilon}_m, T_m) / \beta_\sigma = (\sigma_0)_p f_p(\varepsilon_p, \dot{\varepsilon}_p, T_p)$  always exactly true.

To illustrate the solution explicitly, an example of constitutive equation is presented as follows.

**Example 1.** Consider the Norton–Hoff equation [19, 32]

$$\sigma_d = \sigma_0 e^{n_1} \left( \dot{\varepsilon} / \dot{\varepsilon}_0 \right)^{n_2} \exp(\theta / T), \quad (15)$$

where  $\dot{\varepsilon}_0$  is the corresponding strain-rate for  $\sigma_0$ ;  $n_1$ ,  $n_2$  and  $\theta$  are material constants.

The material numbers (Eqs. (8a), (8b) and (8c)) are derived as

$$Mn\{\varepsilon\} = \frac{E_t \varepsilon}{\sigma_d} = n_1, \quad Mn\{\dot{\varepsilon}\} = \frac{K_t \dot{\varepsilon}}{\sigma_d} = n_2 \quad \text{and} \quad Mn\{T\} = \frac{R_t T}{\sigma_d} = -\frac{\theta}{T}, \quad (16a-c)$$

respectively. It is evident that when the terms of different material effects in the constitutive equation are products, the material number of some effects is only related to its own functional terms.

If  $(n_1)_m = (n_1)_p$ ,  $(n_2)_m = (n_2)_p$  and  $(-\theta_m/T_m) = (-\theta_p/T_p)$ , we obtain

$$\frac{(\varepsilon_m)^{n_1} \left( \dot{\varepsilon}_m / \dot{\varepsilon}_0 \right)^{n_2} \exp(\theta_p/T_p)}{(\varepsilon_p)^{n_1} \left( \dot{\varepsilon}_p / \dot{\varepsilon}_0 \right)^{n_2} \exp(\theta_p/T_p)} = \beta_e^{n_1} \left( \frac{\beta_{\dot{\varepsilon}}}{\beta_{\dot{\varepsilon}_0}} \right)^{n_2} = \text{constant}. \quad (17)$$

The substitution of  $\beta_{\sigma_d} = \beta_\rho \beta_V^{n_1}$ ,  $\beta_e = 1$ ,  $\beta_{\dot{\varepsilon}} = \beta_V / \beta$  (Table 1) and Eq. (17) into Eq. (14) obtains the direct and exact solution as

$$\beta_V = \sqrt{\frac{\beta_{\sigma_0} \beta_e^{n_1} \left( \frac{\beta_{\dot{\varepsilon}}}{\beta_{\dot{\varepsilon}_0}} \right)^{n_2}}{\beta_\rho}} = \sqrt{\frac{\beta_{\sigma_0} \left( \frac{\beta_V}{\beta \beta_{\dot{\varepsilon}_0}} \right)^{n_2}}{\beta_\rho}} \rightarrow \beta_V = \sqrt[2-n_2]{\frac{\beta_{\sigma_0}}{\beta_\rho} \left( \frac{1}{\beta \beta_{\dot{\varepsilon}_0}} \right)^{n_2}} = \text{constant}. \quad (18)$$

Obviously, the correction factor  $\beta_V$  here has nothing to do with the unknown structural responses; and the consistency equality  $(\sigma_0)_m f_m(\varepsilon_m, \dot{\varepsilon}_m, T_m) / \beta_\sigma = (\sigma_0)_p f_p(\varepsilon_p, \dot{\varepsilon}_p, T_p)$  is always exactly true.

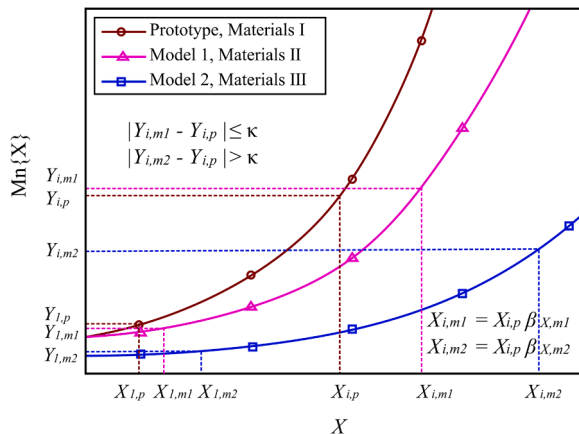


**Fig. 1.** Material II satisfying the similarity criterion  $|\Delta Mn\{X\}| \leq \kappa$  indicates that it is the optimum similitude material for prototype of Material I; while Material III is the non-optimum similitude material.

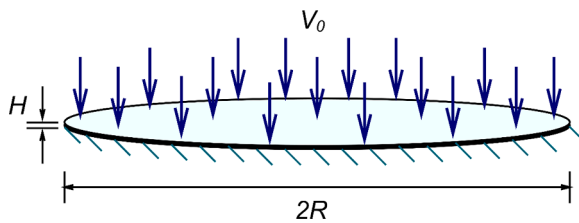


**Fig. 2.** An impacted clamped circular plate with  $R = 0.3\text{ m}$ ,  $H = 0.004\text{ m}$  and  $V_0 = 60\text{ m/s}$ .

#### 2.4. Design scaled model by material similarity curves

The above research proves that the key technique to obtain the direct and exact solution of basic correction factor is to design similarity materials for scaled model. In most cases, it is difficult for two different materials to accurately satisfy the similarity criterion Eq. (7a)-(7c) (i.e.,  $Mn_m\{\varepsilon_m\} = Mn_p\{\varepsilon_p\}$ ,  $Mn_m\{\dot{\varepsilon}_m\} = Mn_p\{\dot{\varepsilon}_p\}$  and  $Mn_m\{T_m\} = Mn_p\{T_p\}$ ). Therefore, by allowing the certain degree errors  $\kappa_1$ ,  $\kappa_2$  and  $\kappa_3$ , the three similarity criterions can be further relaxed.

If we define  $\Delta Mn\{\varepsilon\} = Mn_m\{\varepsilon_m\} - Mn_p\{\varepsilon_p\}$ ,  $\Delta Mn\{\dot{\varepsilon}\} = Mn_m\{\dot{\varepsilon}_m\} - Mn_p\{\dot{\varepsilon}_p\}$  and  $\Delta Mn\{T\} = Mn_m\{T_m\} - Mn_p\{T_p\}$ , they are relaxed as the three inequalities

$$|\Delta Mn\{\varepsilon\}| = |Mn_m\{\varepsilon_m\} - Mn_p\{\varepsilon_p\}| \leq \kappa_1 \quad (19a)$$

(i.e.,  $Mn_p\{\varepsilon_p\} - \kappa_1 \leq Mn_m\{\varepsilon_m\} \leq Mn_p\{\varepsilon_p\} + \kappa_1$ ),

$$|\Delta Mn\{\dot{\varepsilon}\}| = |Mn_m\{\dot{\varepsilon}_m\} - Mn_p\{\dot{\varepsilon}_p\}| \leq \kappa_2 \quad (19b)$$

(i.e.,  $Mn_p\{\dot{\varepsilon}_p\} - \kappa_2 \leq Mn_m\{\dot{\varepsilon}_m\} \leq Mn_p\{\dot{\varepsilon}_p\} + \kappa_2$ )

and

$$|\Delta Mn\{T\}| = |Mn_m\{T_m\} - Mn_p\{T_p\}| \leq \kappa_3 \quad (19c)$$

(i.e.,  $Mn_p\{T_p\} - \kappa_3 \leq Mn_m\{T_m\} \leq Mn_p\{T_p\} + \kappa_3$ ),

respectively. In the three inequalities, it is essential to understand the physical meaning of  $\kappa$ . It should be pointed out that, when  $\Delta Mn\{X\} = 0$ , the correction factor  $\beta_V$  is completely independent of the value of  $\hat{\varepsilon}_p$ ,  $\hat{\dot{\varepsilon}}_p$  and  $\hat{T}_p$  and produces perfectly exact similarity, as verified in Example 1; when  $0 < |\Delta Mn\{X\}| \leq \kappa$ , the factor  $\beta_V$  is not sensitive to their values and produces acceptable exact similarity; while when  $|\Delta Mn\{X\}| > \kappa$ , the factor  $\beta_V$  is more sensitive to their values and the similarity errors could be uncontrollable. Apparently, the physical meaning of  $\kappa$  is the

sensitivity of the correction factor  $\beta_V$  to  $\hat{\varepsilon}_p$ ,  $\hat{\dot{\varepsilon}}_p$  and  $\hat{T}_p$ . Thus, the size of  $\kappa$  controls the errors of  $\beta_V$  for the different values of  $\hat{\varepsilon}_p$ ,  $\hat{\dot{\varepsilon}}_p$  and  $\hat{T}_p$ , which will be verified in Section 3.

To design the similarity materials more intuitively and conveniently, the similarity criterions (Eq. (19a)-(19c)) are plotted in Fig. 1, in which the ‘material number  $Mn\{X\}$  vs.  $X$  (i.e., strain/strain-rate/temperature)’ curves are termed as ‘phase diagram of material similarity’ by the present paper. The quantitative evaluation for material similarity at scaling can be carried out through several discrete points of the material similarity curves. If a material of scaled model satisfies the inequality  $|Mn_m\{X_{i,m}\} - Mn_p\{X_{i,p}\}| \leq \kappa$  ( $i = 1, \dots, N$ ) on the whole, it is considered to be ‘the optimum similitude material’, as the material II in Fig. 1; while, if a material of scaled model doesn’t satisfy the inequality on the whole, it is considered to be ‘the non-optimum similitude material’, as the material III in Fig. 1. In summary,  $\Delta Mn\{X\}$  is the objective metric of the material similarity. The smaller  $|\Delta Mn\{X\}|$  is, the better similarity is; otherwise, the worse.

More interestingly, when  $\beta_X = 1$ , the similarity curves of the optimum similitude materials basically coincide with those of the prototype on the same  $X$  axis; when  $\beta_X \neq 1$ , the similarity curves of the optimum similitude materials basically coincide with those of the prototype on the scaled  $X$  axis (i.e.,  $X/\beta_X$  axis). In addition, when using Fig. 1, the factor  $\beta_X$  needs to be known in advance. For the factor  $\beta_\varepsilon$ ,  $\beta_\varepsilon = 1$  is known. For the factor  $\beta_{\dot{\varepsilon}}$ ,  $\beta_{\dot{\varepsilon}} = \beta_V/\beta$  is unknown since  $\beta_V$  needs to be solved by Eq. (14). In fact, solving  $\beta_V$  is troublesome since  $\beta_V$  is implicitly contained in Eq. (14). For convenience,  $\beta_V$  can be approximated as  $\tilde{\beta}_V =$

$$\sqrt{\frac{\beta_{\varepsilon_0} f_m(\varepsilon_p)}{\beta_p f_p(\varepsilon_p)}} \text{ that ignoring the material strain-rate and temperature effects.}$$

Then,  $\beta_{\dot{\varepsilon}}$  can be approximately estimated as  $\tilde{\beta}_{\dot{\varepsilon}} = \tilde{\beta}_V/\beta$ . For the factor  $\beta_T$ ,  $\beta_T = \beta_V^2/\beta_a$  can be approximately estimated as  $\tilde{\beta}_T = \tilde{\beta}_V^2/\beta_a$ .

Since the optimum similitude material design is determined only according to the coincidence degree of two curves, the proposed material similarity phase diagram is very simple and practical in engineering application.

#### 3. Verification

In this section, numerical simulations of three impacted structures (the circular plate with only strain hardening effects, the crooked plate with the coupling of strain hardening and strain-rate sensitive effects and the Taylor bar with the further consideration of temperature softening effects) of increasing complexity are performed. The constitutive model is set in the three structures by the Johnson-Cook equation (Eq. (B.1)) that is widely used in engineering fields.

To verify the proposed material similarity, the optimum and non-optimum similitude materials (as contrasts) are designed respectively for scaled model, according to Fig. 1. To demonstrate the reasonability of the direct and exact solution when  $\kappa \neq 0$ ,  $\hat{\varepsilon}_p$ ,  $\hat{\dot{\varepsilon}}_p$  and  $\hat{T}_p$  in Eq. (14) are set to different values that having different orders of magnitude. Then, correction factors of velocity are obtained to explore exact similarity of the structural behaviors in the time and space fields.

##### 3.1. Impacted circular plate with only strain hardening materials

To verify material similarity of only strain hardening effects, the impacted structure of a clamped circular plate subjected to impulsive velocity, as shown in Fig. 2, is used.

The clamped circular plate with geometry, impact loads and boundary conditions in Fig. 2 is modeled in the ABAQUS software using the CAX4R axisymmetric elements and discretized with 600 elements in radius and 8 elements in thickness direction. The Nickel 200 in Table B.1 is used in here as the prototype material. For scaled models, all geometric sizes are scaled by  $\beta = 1/100$ . The impact loads of impulsive

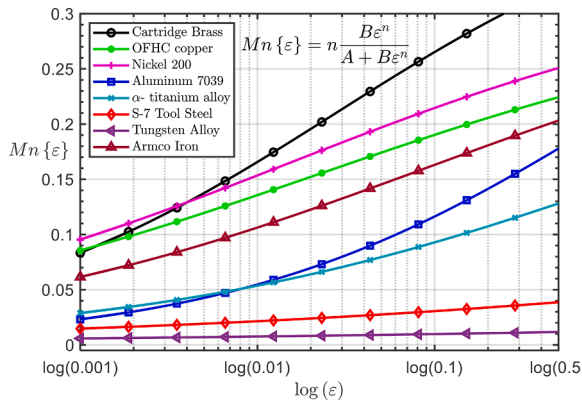


Fig. 3. Material similarity phase diagram of the strain hardening effects.

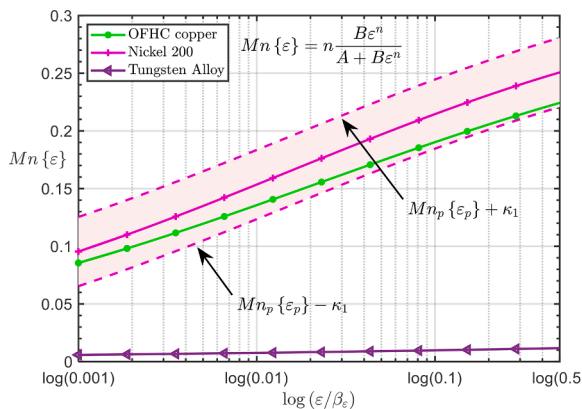


Fig. 4. The material similarity phase diagram of strain hardening effects shows that when Nickel is the prototype material, Copper satisfies the similarity criterion Eq. (19a) while Tungsten does not.

Table 2

The  $\Delta Mn\{\epsilon\}$  values for scaled circular plates.  $\Delta Mn\{\epsilon\} = Mn_m\{\epsilon_m\} - Mn_p\{\epsilon_p\}$  and  $\epsilon_m = \beta_\epsilon \epsilon_p$ .

Discrete points	Material	$\Delta Mn\{\epsilon\}$	Material	$\Delta Mn\{\epsilon\}$
$\epsilon_p = 0.001$	Tungsten	-0.090	Copper	-0.010
$\epsilon_p = 0.01$	Tungsten	-0.146	Copper	-0.018
$\epsilon_p = 0.5$	Tungsten	-0.239	Copper	-0.026

velocity are scaled by the correction factor  $\beta_V$ . The material and the factor  $\beta_V$  used for scaled models are introduced in detail in the following content. In addition, in order to eliminate the interference of similarity errors of elasticity, the elastic modulus  $E^e$  is set to 10000 times of  $\sigma_0$  to precisely satisfy the proposed elastoplastic similarity condition  $(\sigma_0/E^e)_m / (\sigma_0/E^e)_p = \beta_\epsilon$  in Section 2.1. In actual scaling tests, elastic similarity can be included by looking for materials that satisfy the elastoplastic similarity condition as much as possible. Nevertheless, this paper focuses on the similarity of plasticity, and further research on this important issue is necessary in the future.

### 3.1.1. Formulation for impacted circular plate

When only the strain hardening effects are considered, the Johnson-Cook equation Eq. (B.1) is simplified to  $\sigma_d = A + Be^n$ . The substitution of  $E_t(\epsilon) = \partial\sigma_d/\partial\epsilon = nBe^{n-1}$  into Eq. (8a) obtains

$$Mn\{\epsilon\} = \frac{E_t\epsilon}{\sigma_d} = n \frac{Be^n}{A + Be^n}. \quad (20)$$

The material similarity is evaluated in Fig. 3 with eight different materials in Table B.1. Apparently, the curve of OFHC copper is closest to the curve of Nickel 200, while curve of Tungsten Alloy is furthest from the curve of Nickel 200. When the factor  $\beta_\epsilon = 1$  is used, according to the principle shown in Fig. 1, OFHC copper is the optimum similitude material; while, Tungsten Alloy is the non-optimum similitude material. As the most typical representative of optimum and non-optimum similitude materials in the eight different materials, OFHC copper and Tungsten Alloy are selected intuitively in the scaled models, respectively.

In order to further quantitatively evaluate the similarity results of the selected materials, Eq. (19a) in the strain window [0, 0.5] is carried out. The window is wide enough and can well cover the variation range of strain of impacted circular plate prototype, which can be verified by subsequent calculations in Section 3.1.2. It should be noted that although a better optimum similitude material could be obtained when using the precise strain window, which happens to contain the structural strain response, it is difficult to know the response before scaling tests. Therefore, in general, a fixed and wide window can be used for material similarity design. The error margin  $\kappa_1$  is assumed to be 0.03 which is about one tenth of the maximum vertical coordinate of Fig. 3. Then, for Copper, Nickel and Tungsten, the similarity criterion Eq. (19a) (i.e.,  $Mn_p\{\epsilon_p\} - \kappa_1 \leq Mn_m\{\epsilon_m\} \leq Mn_p\{\epsilon_p\} + \kappa_1$ ) is intuitively plotted in Fig. 4. The optimum similitude material Copper is inside the accepted difference of  $\kappa_1 = 0.03$ , while the non-optimum similitude material Tungsten is outside. Furthermore, the  $\Delta Mn\{\epsilon\}$  values, which are used to quantitatively evaluate the material similarity of scaled models, are listed in Table 2. Obviously, 0.03 for  $\kappa_1$  can make the significant difference between the optimum and non-optimum similitude materials. In addition, in combination with Fig. A.1, it can be found that the predicted flow stress of the Copper always approximates to the prototype Nickel at different orders of magnitude of strain, thus overcoming the inexact defect of previous method.

To verify the direct and exact property of Eq. (14) used optimum and non-optimum similitude materials,  $\hat{\epsilon}_p = 0.005, 0.01, 0.05, 0.1$  and  $0.2$  are studied. Finally, scaled models with the basic scaling factors  $\beta$ ,  $\beta_p$  and  $\beta_V$  are listed in Table 3. From  $\hat{\epsilon}_p = 0.005$  to  $0.2$ , the correction factor  $\beta_V$  for Tungsten changed by -28 percent; while, for Copper, it only changed by -4 percent, which further verifies the conclusion of Eq. (14) — for the optimum similitude materials,  $\beta_V$  is not sensitive to the value of  $\hat{\epsilon}_p$ ; for the non-optimum similitude materials,  $\beta_V$  is very sensitive to the value of  $\hat{\epsilon}_p$ . Since the correction factor for Copper does not vary significantly, it is appropriate to design the optimum similitude materials using  $\kappa_1 = 0.03$ .

### 3.1.2. Results for impacted circular plate

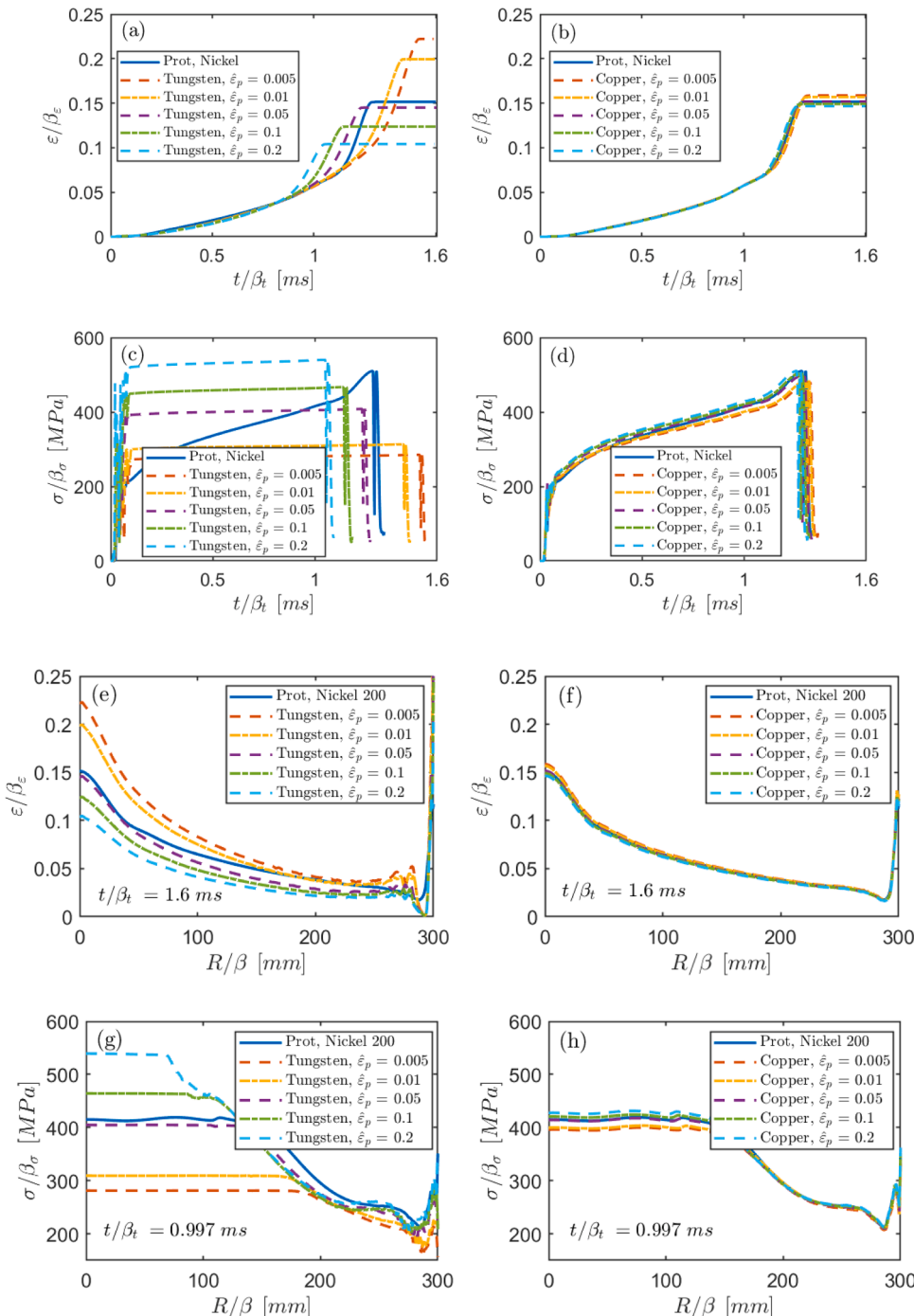
The refined evaluation of similarity in time and space fields by the strain and stress responses is plotted in Fig. 5. For the scaled models with the non-optimum similitude material Tungsten, the strain and stress responses deviate significantly from the prototype responses, Fig. 5a, c, e and g. And the predicted results are very sensitive to the value of  $\hat{\epsilon}_p$ . However, for the optimum similitude material Copper, the strain and stress responses of scale models are almost exactly consistent with those of the prototype, Fig. 5b, d, f and h. And the predicted results are basically unaffected by  $\hat{\epsilon}_p$ .

Further evaluation of similarity in time and space fields by the displacement responses is shown in Fig. 6. The responses of the non-optimum similitude material Tungsten are very sensitive to the value of  $\hat{\epsilon}_p$  and lead to significant predicted errors (maximum error being 19 percent) for prototype, Fig. 6a and c. However, the optimum similitude material Copper responses are always nearly the same as the prototype responses, only with the maximum error 0.2 percent, Fig. 6b and d. In addition, the average strain [33] can be obtained as  $\bar{\epsilon}_p = \frac{\rho V_0^2}{3\sigma_0} = 0.066$ . It can be found that, when  $\hat{\epsilon}_p \rightarrow \bar{\epsilon}_p$ , the predicted responses are closest to the prototype both for non-optimum and optimum similitude material,

**Table 3**

Three basic scaling factors for circular plate.

Scaled model	Material	$\beta$	$\beta_p$	$\beta_V$	Scaled model	Material	$\beta$	$\beta_p$	$\beta_V$
1 ( $\hat{\epsilon}_p = 0.005$ )	Tungsten	0.01	1.910	1.743	6 ( $\hat{\epsilon}_p = 0.005$ )	Copper	0.01	1.007	0.726
2 ( $\hat{\epsilon}_p = 0.01$ )	Tungsten	0.01	1.910	1.662	7 ( $\hat{\epsilon}_p = 0.01$ )	Copper	0.01	1.007	0.722
3 ( $\hat{\epsilon}_p = 0.05$ )	Tungsten	0.01	1.910	1.453	8 ( $\hat{\epsilon}_p = 0.05$ )	Copper	0.01	1.007	0.711
4 ( $\hat{\epsilon}_p = 0.1$ )	Tungsten	0.01	1.910	1.357	9 ( $\hat{\epsilon}_p = 0.1$ )	Copper	0.01	1.007	0.705
5 ( $\hat{\epsilon}_p = 0.2$ )	Tungsten	0.01	1.910	1.261	10 ( $\hat{\epsilon}_p = 0.2$ )	Copper	0.01	1.007	0.699

**Fig. 5.** Impact responses of the center point (a-d) and the neutral surface (e-h) of circular plates with the non-optimum similitude material Tungsten and the optimum similitude material Copper.

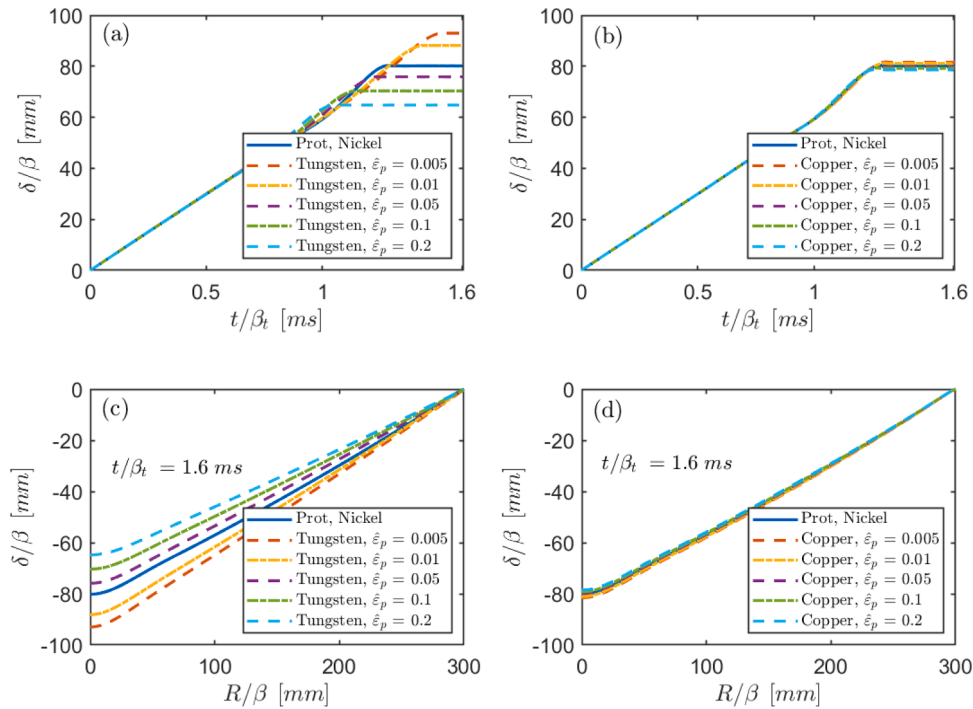


**Fig. 6.** Displacement responses of the center point (a-b) and the neutral surface (c-d) of circular plates with the non-optimum similitude material Tungsten and the optimum similitude material Copper.

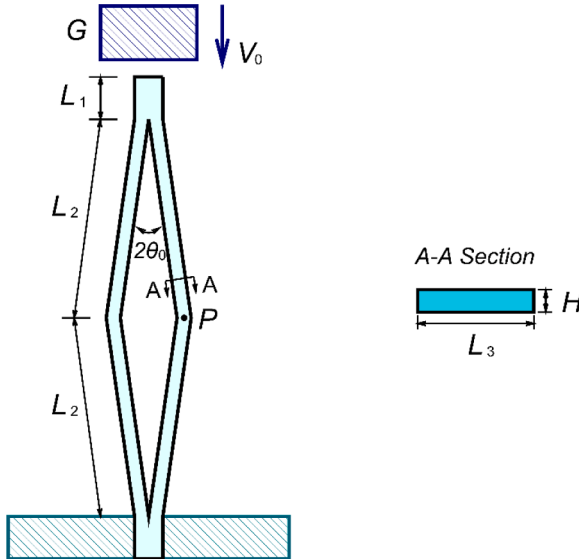


**Fig. 7.** Crooked plates under axial impact with  $L_1 = 0.005$  m,  $L_2 = 0.025$  m,  $L_3 = 0.051$  m,  $H = 0.0016$  m,  $\theta_0 = 1.6^\circ$ ,  $G_p = 4$  kg and  $V_0 = 12$  m /s.

Figs. 5 and 6. Therefore, selecting  $\hat{\varepsilon}_p$  which is close to the average strain helps to reduce the similarity errors since the average means that one part of the error compensates for another part of the error. But for Fig. 5c, the similarity errors are still very significant, which indicates that the use of optimum similitude materials is necessary for more refined exact similarity.

### 3.2. Impacted crooked plate with both strain hardening and strain-rate sensitive materials

To verify material similarity of both the strain hardening effects and the strain-rate sensitive effects, a more complicated structure of two pre-

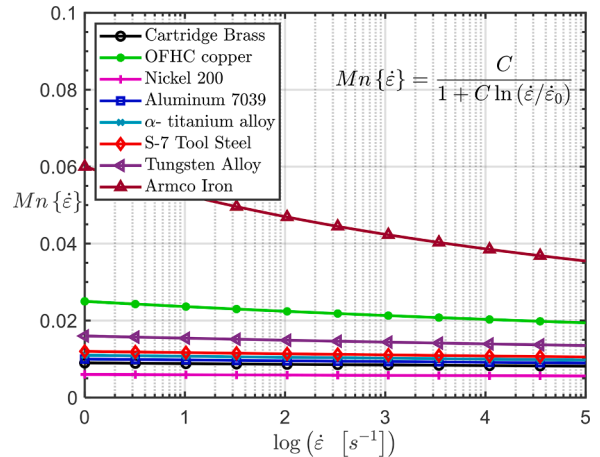


**Fig. 8.** Material similarity phase diagram of the strain-rate sensitive effects.

bent plates (clamped together at both ends) with the initial crooked angle and subjected to an axial impact mass, as shown in Fig. 7, is used. The structure is classified as ‘type II’ that being very sensitive to impact velocity [4] and therefore more suitable to reflect strain-rate sensitive effects. Its motion is divided into two phases, a rapid compression of the plates and a subsequent bending along the initial crooked angles [4, 14, 19, 28].

The crooked plate with geometry, impact loads and boundary conditions in Fig. 7 is modeled in the ABAQUS software using the CPE4R elements and discretized with 25 elements in  $L_1$ , 125 elements in  $L_2$  and 8 elements in thickness  $H$  direction. The Tungsten Alloy in Table B.1 is used in here as the prototype material. For scaled models, all geometric sizes are scaled by  $\beta = 1/10$ . The impact mass is modelled as a steel mass block with the Analytical Rigid. The contact between the impact mass and the plate uses the ‘Surface to Surface contact’. The impact velocity and mass are scaled by the correction factor  $\beta_V$  and the scaling factor

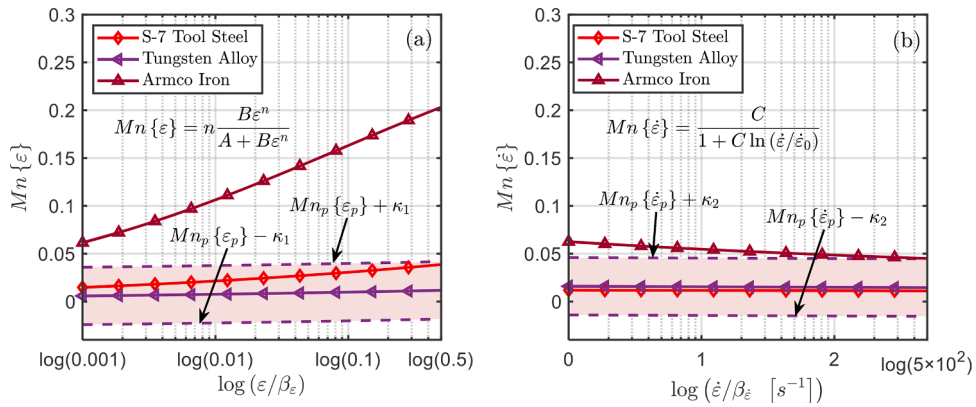


**Fig. 9.** The material similarity phase diagram of strain hardening effects (a) and strain-rate sensitive effects (b) shows that when Tungsten is the prototype material, S-7 simultaneously satisfies the similarity criterions Eqs. (19a) and (19b) while Iron does not.

**Table 4**

The  $\Delta Mn$  values for scaled crooked plate.  $\Delta Mn\{\epsilon\} = Mn_m\{\epsilon_m\} - Mn_p\{\epsilon_p\}$ ,  $\epsilon_m = \beta_e \epsilon_p$  and  $\beta_e = 1$ ;  $\Delta Mn\{\dot{\epsilon}\} = Mn_m\{\dot{\epsilon}_m\} - Mn_p\{\dot{\epsilon}_p\}$ ,  $\dot{\epsilon}_m = \beta_e \dot{\epsilon}_p$ ,  $\beta_e \approx \tilde{\beta}_e = \frac{1}{\beta} \sqrt{\frac{\beta_{\sigma_0}}{\beta_\rho}}$  = 1.49 for S-7 and 0.50 for Iron.

Discrete points	Material	$\Delta Mn$	Material	$\Delta Mn$
$\epsilon_p = 0.001$	Iron	0.056	S-7	0.009
$\epsilon_p = 0.01$	Iron	0.099	S-7	0.014
$\epsilon_p = 0.5$	Iron	0.192	S-7	0.027
$\dot{\epsilon}_p = 1 \text{ s}^{-1}$	Iron	0.039	S-7	-0.004
$\dot{\epsilon}_p = 10 \text{ s}^{-1}$	Iron	0.033	S-7	-0.004
$\dot{\epsilon}_p = 500 \text{ s}^{-1}$	Iron	0.026	S-7	-0.004

$\beta_G = \beta_\rho \beta^3$ , respectively. The material and the basic factor  $\beta_V$  and  $\beta_\rho$  used for scaled models are described in detail in the following content. The setting method of elasticity is the same as that in Section 3.1.

### 3.2.1. Formulation for impacted crooked plate

When both the strain hardening effects and the strain-rate sensitive effects are fully considered, the Johnson-Cook equation Eq. (B.1) is simplified to  $\sigma_d = (A + Be^n)(1 + Cln(\dot{\epsilon}/\dot{\epsilon}_0))$ . The substitution of  $E_t(\epsilon, \dot{\epsilon}) = \partial \sigma_d / \partial \epsilon = Bne^{n-1}(1 + Cln(\dot{\epsilon}/\dot{\epsilon}_0))$  into Eq. (8a) and the substitution of  $K_t(\epsilon, \dot{\epsilon}) = \partial \sigma_d / \partial \dot{\epsilon} = (A + Be^n)(C/\dot{\epsilon})$  into Eq. (8b) obtain the material numbers as

$$Mn\{\epsilon\} = \frac{E_t \epsilon}{\sigma_d} = n \frac{Be^n}{A + Be^n} \quad \text{and} \quad Mn\{\dot{\epsilon}\} = \frac{C}{1 + Cln\left(\frac{\dot{\epsilon}}{\dot{\epsilon}_0}\right)}, \quad (21\text{a-b})$$

respectively. It is evident from Eqs. (20) and (21) that the numbers  $Mn\{\epsilon\}$  and  $Mn\{\dot{\epsilon}\}$  are independent of each other, just like Eq. (16a) and Eq. (16b). Therefore, the material similarity of different effects can be evaluated independently.

The material similarity is evaluated by ‘material number – strain’

**Table 5**

Three basic scaling factors for crooked plate.

Scaled model ( $\hat{\epsilon}_p, \hat{\dot{\epsilon}}_p$ )	Material	$\beta$	$\beta_\rho$	$\beta_V$	Scaled model ( $\hat{\epsilon}_p, \hat{\dot{\epsilon}}_p$ )	Material	$\beta$	$\beta_\rho$	$\beta_V$
1 (0.005, 10 s⁻¹)	Iron	0.1	0.464	0.630	6 (0.005, 10 s⁻¹)	S-7	0.1	0.456	1.555
2 (0.005, 500 s⁻¹)	Iron	0.1	0.464	0.668	7 (0.005, 500 s⁻¹)	S-7	0.1	0.456	1.543
3 (0.05, 250 s⁻¹)	Iron	0.1	0.464	0.752	8 (0.05, 250 s⁻¹)	S-7	0.1	0.456	1.572
4 (0.2, 10 s⁻¹)	Iron	0.1	0.464	0.799	9 (0.2, 10 s⁻¹)	S-7	0.1	0.456	1.605
5 (0.2, 500 s⁻¹)	Iron	0.1	0.464	0.846	10 (0.2, 500 s⁻¹)	S-7	0.1	0.456	1.593

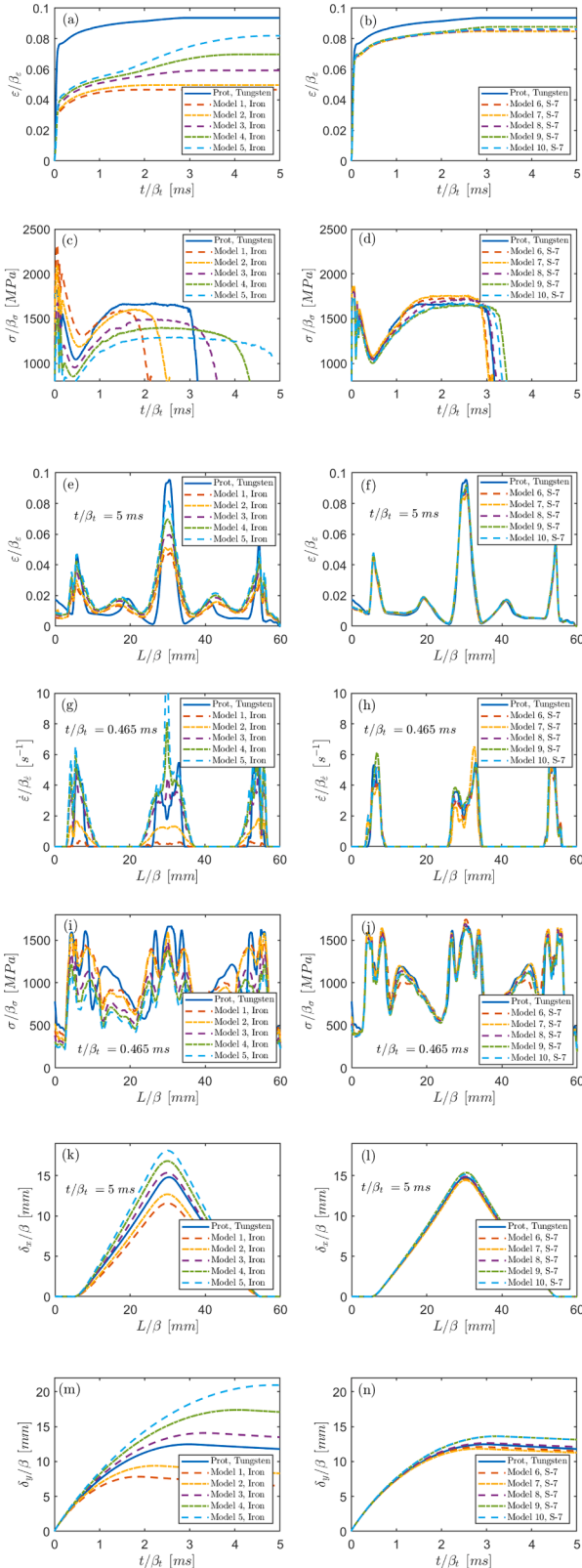


**Fig. 10.** Impact responses of the point P (a-d), the neutral surface of plate (e-l) and the impact mass (m-n) of crooked plates with the optimum similitude material S-7 and the non-optimum similitude material Iron.

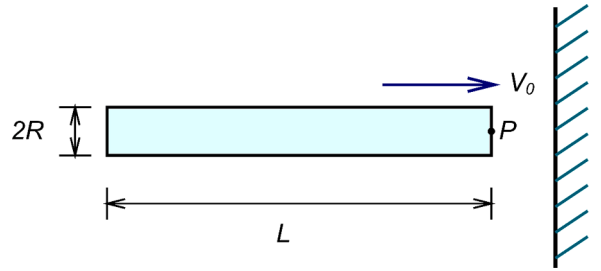


**Fig. 11.** Taylor bar of  $L = 31.75 \times 10^{-3}$  m,  $R = 3.17 \times 10^{-3}$  m and  $V_0 = 200$  m/s impacting a rigid wall.

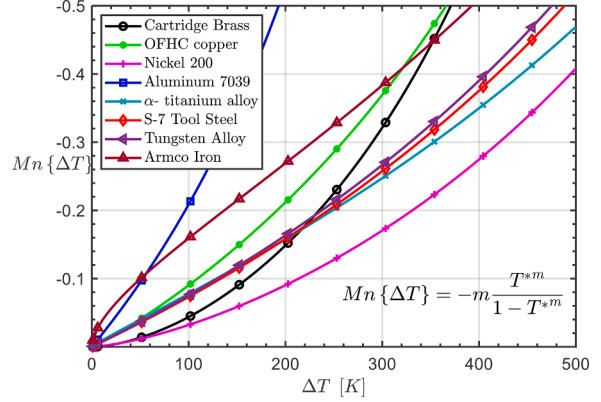


**Fig. 12.** Material similarity phase diagram of the temperature softening effects

To verify the direct and exact property of Eq. (14) used the optimum and non-optimum similitude materials,  $(\hat{\varepsilon}_p, \hat{\dot{\varepsilon}}_p) = (0.005, 10 s^{-1})$ ,  $(0.005, 500 s^{-1})$ ,  $(0.05, 250 s^{-1})$ ,  $(0.2, 10 s^{-1})$  and  $(0.2, 500 s^{-1})$  are studied. Finally, scaled models with the basic scaling factors  $\beta$ ,  $\beta_p$  and  $\beta_V$  are listed in Table 5. From  $\hat{\varepsilon}_p = 0.005$  to 0.2 (when  $\hat{\dot{\varepsilon}}_p = 10 s^{-1}$ ), the factor  $\beta_V$  for Iron changed by 27 percent; while, for S-7, it only changed by 3 percent. From  $\hat{\varepsilon}_p = 10 s^{-1}$  to 500  $s^{-1}$  (when  $\hat{\dot{\varepsilon}}_p = 0.2$ ), the factor  $\beta_V$  for Iron changed by 6 percent; while, for S-7, it only changed by -1 percent, which further verifies the conclusion of Eq. (14) — for the optimum similitude materials,  $\beta_V$  is not sensitive to the value of  $\hat{\varepsilon}_p$ ; for the non-optimum similitude materials,  $\beta_V$  is more sensitive to the value of  $\hat{\varepsilon}_p$ . Since the correction factor for S-7 does not vary significantly, it is appropriate to design the optimum similitude materials using  $\kappa_1 = 0.03$  and  $\kappa_2 = 0.03$ .

### 3.2.2. Results for impacted crooked plate

The refined evaluation of similarity in time and space fields by the strain, strain-rate, stress and displacement responses is plotted in Fig. 10. The responses of the non-optimum similitude material Iron are very sensitive to the value of  $\hat{\varepsilon}_p$  and  $\hat{\dot{\varepsilon}}_p$  and have significant predicted errors, and even failed prediction, Fig. 10a, c, e, g, i, k and m. However, the optimum similitude material S-7 responses are always nearly the same as the prototype responses, Fig. 10b, d, f, h, j, l and n. Although there are some small errors, it is considered acceptable for almost exact similarity. From Fig. 10m to Fig. 10n, the maximum displacement prediction error of the impact mass is also effectively reduced from 68 percent to the current 9 percent. The results show once more that the present method after using the optimum similitude material obtains direct and acceptable exact prediction when the strain hardening effects and strain-rate sensitive effects are coupled together.

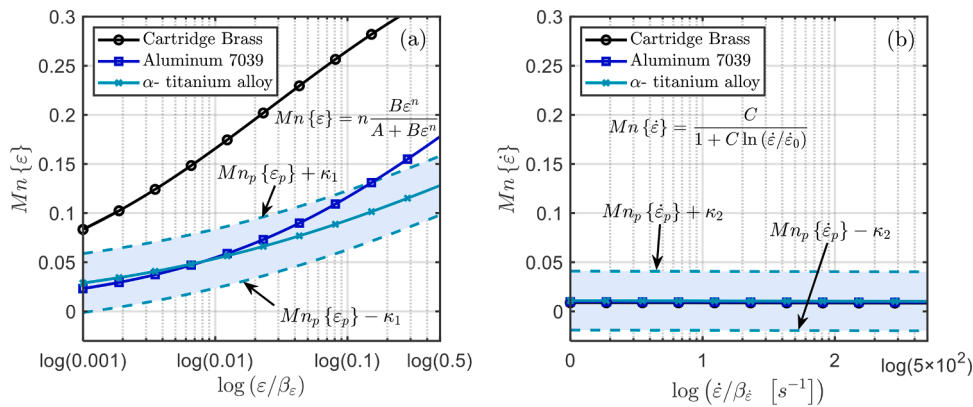


**Fig. 13.** The material similarity phase diagram of strain hardening effects (a) and strain-rate sensitive effects (b) shows that when Titanium is the prototype material, Aluminum simultaneously satisfies the similarity criterions Eqs. (19a) and (19b) on the whole, while Brass does not.

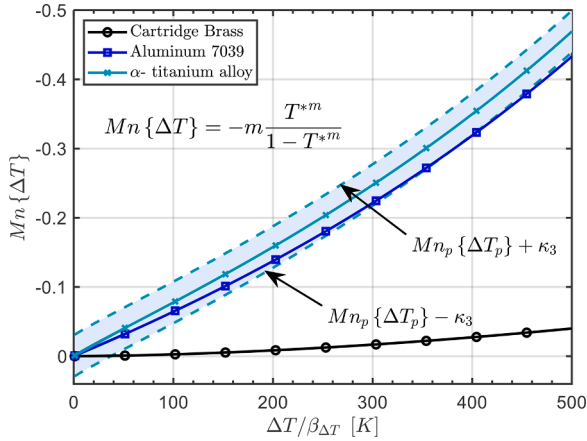


**Fig. 14.** The material similarity phase diagram of temperature softening effects shows that when Titanium is the prototype material, Aluminum satisfies the similarity criterions Eq. (19c) on the whole, while Brass does not.

**Table 6**

The  $\Delta Mn\{\Delta T\}$  values for scaled circular plates.  $\Delta Mn\{\Delta T\} = Mn_m\{\Delta T_m\} - Mn_p\{\Delta T_p\}$ ,  $\Delta T_m = \beta_{\Delta T} \Delta T_p$ ,  $\beta_{\Delta T} \approx \tilde{\beta}_{\Delta T} = 0.35$  (Aluminum) and 0.19 (Brass).

Discrete points	Material	$\Delta Mn\{\Delta T\}$	Material	$\Delta Mn\{\Delta T\}$
$\Delta T_p = 1$ K	Brass	0.009	Aluminum	0.003
$\Delta T_p = 200$ K	Brass	0.150	Aluminum	0.020
$\Delta T_p = 500$ K	Brass	0.431	Aluminum	0.034

### 3.3. Impacted Taylor bar with thermal softening materials

The temperature softening effects due to the heat produced by the consumed plastic deformation work is important in high velocity impact problems [6, 34]. To further verify its similarity, a typical impact model of Taylor bar impacting a rigid wall, as shown in Fig. 11, is carried out here.

The Taylor bar with geometry, impact loads and boundary conditions in Fig. 11 is modeled in the ABAQUS software using the CAX4R axisymmetric elements and discretized with 100 elements in  $L$  and 16 elements in  $R$  direction. The α-titanium alloy in Table B.1 is used in here as the prototype material. For scaled models, all geometric sizes are scaled by  $\beta = 1/10$ . The impact velocity of Taylor bar is scaled by the correction factor  $\beta_V$ . The material and the factor  $\beta_V$  used for scaled models are described in detail in the following content. For prototype and scaled models, the rigid wall is simulated by a circular plate of rigid. The contact between the Taylor bar and the plate used general contact and the friction coefficient is set as 0.047 [35]. The work rate to heat rate

conversion fraction  $\zeta$  is set to be 0.9 [25]. The setting method of elasticity is the same as that in Section 3.1.

#### 3.3.1. Formulation for impacted Taylor bar

When the correction method of temperature is applied, correcting the initial temperature means that the applicable conditions  $T \geq T_r$  ( $T_r$  is usually room temperature  $T_0 = 298K$  in most cases) of the Johnson-Cook model could be broken. To overcome this defect in the previous correction methods, we use the adiabatic temperature rise  $\Delta T = T - T_r$  as a new variable instead of the variable  $T$  in Eqs. (1)-(19). Then, the scaling relation of the specific heat  $\alpha$  in Table 1,  $\beta_\alpha = \beta_V^2/\beta_T$ , is modified as  $\beta_\alpha = \beta_\zeta \beta_V^2/\beta_{\Delta T}$ <sup>2</sup>. Since there is no need to correct the initial temperature, this modified technique has special advantages in the impact experiment.

When the Johnson-Cook equation is used to further consider the temperature softening effects, the material number of temperature rise is expressed as

$$Mn\{\Delta T\} = \frac{R_t \Delta T}{\sigma_d} = -m \frac{T^{*m}}{1 - T^{*m}}, \quad (22)$$

where  $R_t = \partial \sigma_d / \partial \Delta T = -(A + Be^n)(1 + Cln(\dot{\varepsilon}/\dot{\varepsilon}_0))[mT^{*m-1}(1/(T_m - T_r))]$ . Then, the material similarity is independently evaluated by ‘material number – strain’ phase diagram (Fig. 3), ‘material number – strain-rate’ phase diagram (Fig. 8) and ‘material number – temperatures rise’ phase diagram (as shown in Fig. 12) with eight different materials in Table B.1.

When designing optimum similitude materials, it is difficult to satisfy all three similarity criteria (Eqs. (19a)–(19c)) simultaneously. Therefore, according to the research problem, when one of the material effects is more correlated, its similarity criterion should be satisfied first. For the impacted Taylor bar, all three material effects could be important because of its high impact velocity and large plastic deformation. To begin with, the relatively simple similarity evaluation of strain hardening and strain-rate effects is performed. Similar to Section 3.2.1, according to the coincidence of the curves, it can be intuitively designed that the optimum similitude material is Aluminum 7039 from Fig. 3 and Fig. 8. The non-optimum similitude material is designed as Cartridge Brass. Then, for Brass, Aluminum and Titanium, the similarity criterions Eq. (19a) (i.e.,  $Mn_p\{\dot{\varepsilon}_p\} - \kappa_1 \leq Mn_m\{\dot{\varepsilon}_m\} \leq Mn_p\{\dot{\varepsilon}_p\} + \kappa_1$ ) and Eq. (19b) (i.e.,  $Mn_p\{\dot{\varepsilon}_p\} - \kappa_2 \leq Mn_m\{\dot{\varepsilon}_m\} \leq Mn_p\{\dot{\varepsilon}_p\} + \kappa_2$ ) are plotted in Fig. 13. The values of  $\kappa_1$  and  $\kappa_2$  are both taken to 0.03. The scaling factors used in

<sup>2</sup> The adiabatic temperature rise [34] is defined as  $\Delta T = \frac{\zeta}{\rho\alpha} \int_0^e \sigma de$ . Therefore, its scaling relationship can be derived as  $\beta_{\Delta T} = \beta_\zeta \beta_\alpha \beta_e / \beta_\rho \beta_{\alpha 0} = \beta_\zeta \beta_V^2 / \beta_\alpha$  when  $\beta_\sigma = \beta_\rho \beta_V^2$  and  $\beta_e = 1$  in Table 1 are used.

**Table 7**  
Four basic scaling factors for Taylor bar.

Scaled model	Material	$\beta$	$\beta_\rho$	$\beta_V$	$\beta_{\Delta T}$	Scaled model	Material	$\beta$	$\beta_\rho$	$\beta_V$	$\beta_{\Delta T}$
1 ( $\Delta \hat{T}_p = 10$ )	Brass	0.1	1.889	0.391	0.187	5 ( $\Delta \hat{T}_p = 10$ )	Aluminum	0.1	0.614	0.814	0.356
2 ( $\Delta \hat{T}_p = 150$ )	Brass	0.1	1.889	0.413	0.208	6 ( $\Delta \hat{T}_p = 150$ )	Aluminum	0.1	0.614	0.822	0.363
3 ( $\Delta \hat{T}_p = 300$ )	Brass	0.1	1.889	0.436	0.232	7 ( $\Delta \hat{T}_p = 300$ )	Aluminum	0.1	0.614	0.825	0.366
4 ( $\Delta \hat{T}_p = 500$ )	Brass	0.1	1.889	0.470	0.269	8 ( $\Delta \hat{T}_p = 500$ )	Aluminum	0.1	0.614	0.827	0.367

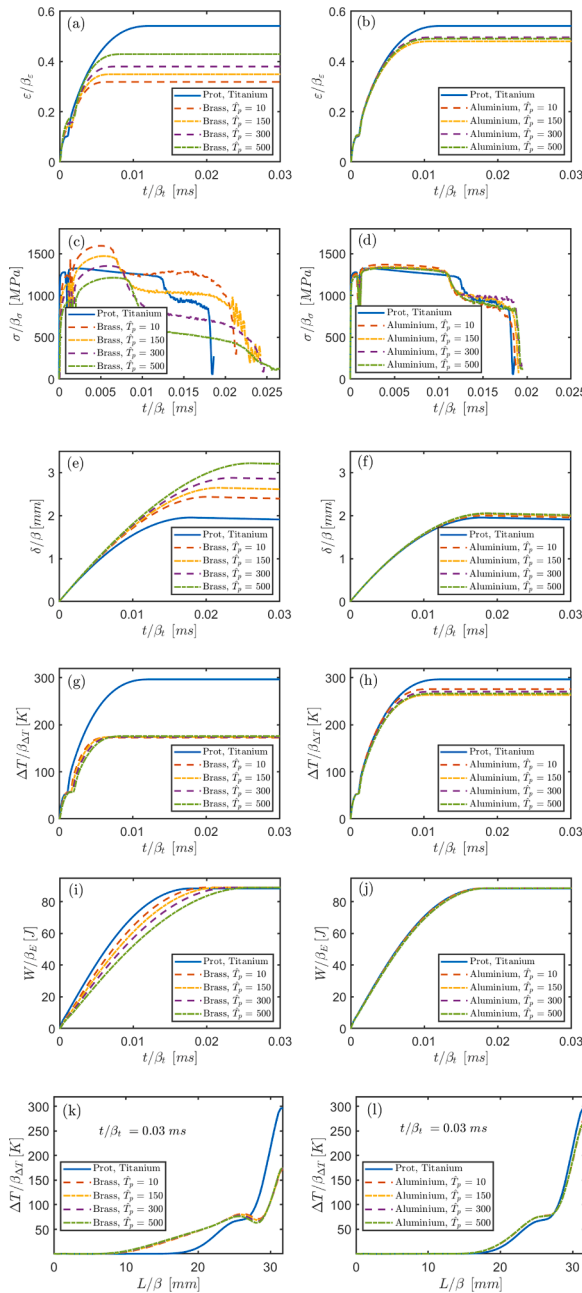


**Fig. 15.** Impact responses of the point P (a-h), all elements (i-j) and the central axis of bar (k-l) of Taylor bar with the non-optimum similitude material Brass and the optimum similitude material Aluminum.

**Fig. 13a and b** are respectively  $\beta_e = 1$ ,  $\beta_{\dot{\varepsilon}} \approx \tilde{\beta}_V/\beta = 8.1$  (Aluminum) and 3.9 (Brass), where  $\tilde{\beta}_V = \sqrt{\frac{\beta_{a_0}}{\beta_p} \frac{f_m(\epsilon_p=0.2)}{f_p(\epsilon_p=0.2)}} = \sqrt{\frac{1}{\beta_p} \frac{A_m + B_m \times 0.2^m}{A_p + B_p \times 0.2^p}} = 0.81$  (Aluminum) and 0.39 (Brass). Obviously, the Aluminum basically satisfies both Eq. (19a) and Eq.(19b), while, the Brass only satisfies Eq. (19b) but not Eq. (19a).

Secondly, the similarity of the temperature-softening effects of the two materials is further examined. The approximate factor  $\tilde{\beta}_{\Delta T}$  used for Fig. 1 is calculated as  $\tilde{\beta}_{\Delta T} = \beta_s \tilde{\beta}_V^2 / \beta_a = 0.35$  (Aluminum) and 0.19 (Brass), respectively. Then, Eq. (19c) in the temperature rise window [0, 500 K] is carried out respectively when  $\kappa_3$  is also assumed to be 0.03. The window is wide enough and can well cover the variation range of temperature rise of impacted Taylor bar prototype, which can be verified by subsequent calculations in Section 3.3.2. For Brass, Aluminum and Titanium, the similarity criterion Eq. (19c) (i.e.,  $Mn_p\{\Delta T_p\} - \kappa_3 \leq Mn_m\{\Delta T_m\} \leq Mn_p\{\Delta T_p\} + \kappa_3$ ) is intuitively plotted in Fig. 14. The optimum similitude material Aluminum is inside the accepted difference of  $\kappa_3 = 0.03$ , while the non-optimum similitude material Brass is outside. Furthermore, the  $\Delta Mn\{\Delta T\}$  values, which are used to quantitatively evaluate the material similarity of scaled models, are listed in Table 6. The Aluminum further basically satisfies the similarity criterion Eq. (19c); while, Brass does not meet.

Finally, to verify the direct and exact property of Eq. (14) used the optimum and non-optimum similitude materials,  $\Delta \hat{T}_p = 10, 150, 300, 500$  K are studied. The strain and strain-rate are set as  $\hat{\epsilon}_p = 0.2$  and  $\hat{\dot{\epsilon}}_p = 1E4$  s<sup>-1</sup> respectively for the Taylor bar prototype of high velocity impact. Scaled models with the basic scaling factors  $\beta$ ,  $\beta_\rho$ ,  $\beta_V$  and  $\beta_{\Delta T}$  are listed in Table 7. From  $\Delta \hat{T}_p = 10$  to 500 K, the factor  $\beta_V$  for Brass changed by 20 percent; while, for Aluminum, it only changed by 2 percent, which further verifies the conclusion of Eq. (14) — for the optimum similitude materials,  $\beta_V$  is not sensitive to the value of  $\Delta \hat{T}_p$ . Since the correction factor for Aluminum does not vary significantly, it is appropriate to design the optimum similitude materials using  $\kappa_3 = 0.03$ .

### 3.3.2. Results for impacted Taylor bar

The refined evaluation of similarity in time and space fields by the strain, stress, displacement temperature rise, plastic dissipation energy (W) is plotted in Fig. 15. The response of the non-optimum similitude material Brass is very sensitive to the value of  $\Delta \hat{T}_p$  and leads to failed predictions, Fig. 15a, c, e, g, i and k. However, the optimum similitude material Aluminum responses are always nearly the same as the prototype responses, Fig. 15b, d, f, h, j and l. From Fig. 15e to Fig. 15f, the maximum displacement prediction error is also effectively reduced from 67 percent to the current 4 percent. The results show once more that the present method after using the optimum similitude material obtains direct and acceptable exact prediction when the strain hardening effects, strain-rate sensitive effects and temperature softening effects are coupled together.

#### 4. Conclusion

This paper proposed a material similarity framework for strain hardening, strain-rate sensitive and temperature softening solid materials. It is defined what is the optimum similitude materials of solid mechanics and how to design the optimum similitude materials at scaling. As a result, the inherent non-direct and inexact defects, existing in all previous similarity theory of structural impact when using the basic correction factors, are overcome fundamentally. Since the proposed material similarity is an important property for the most basic material stress - strain/strain-rate/temperature relations, it must be respected in solid scaling experiments. Compared with previous works about scaling that only focus on the correction methods of initial conditions, the new proposed method is mainly reflected in five aspects.

- (1) Based on the similarity analysis of the total differential relation of the thermo-visco-plastic constitutive equation, the material dimensionless numbers of strain hardening, strain-rate sensitivity and temperature softening effects are derived, which reflect the intrinsic requirement of similarity theory for material basic mechanical properties. For the product form of constitutive model, the material numbers of different effects are independent of each other, and only related to the constitutive parameters of the correlation effect, which provides a particular advantage for the independent evaluation of different material effects.
- (2) Phase diagram of 'Material numbers - strain/strain-rate/temperature' curves are further proposed to evaluate material similarity at scaling. When carrying out the scaled solid mechanic experiments, it is very intuitive and convenient to design the optimum similitude materials according to the coincidence degree of the curves between scaled model and the prototype. Studies using the Johnson-Cook constitutive model and relatively simple impact models further indicate that, for material similarity phase diagram, the error margins  $\kappa_1, \kappa_2, \kappa_3 \approx 0.03$  in Fig. 1 can better quantitatively design the optimum similitude materials at scaling. For more complicated impact models, the value of  $\kappa$  needs to be further verified in the future.
- (3) The universal direct and exact solution of the basic correction factors in similarity theory is proved theoretically based on the existence condition that the material numbers in the prototype and the scaled model are equal. Although the velocity correction factor is taken as an example in this paper, the proposed direct and exact solution is also applicable to other correction methods such as density and geometric thickness developed in the past. Since this solution has unique advantages of being independent of the structural strain, strain-rate and temperature responses, the previous inherent non-direct and inexact difficulty is overcome radically.

- (4) By using the optimum similitude material to design scaled model and prototype, different materials of strain hardening, strain-rate sensitive and thermal softening effects are verified to have acceptable exact similarity in the time and space fields by three relatively simple numerical impacted models, no matter the displacement responses or the stress, strain, strain-rate and temperature responses. However, when using the non-optimum similitude material, the similarity errors are not controllable and usually could lead to failed prediction. This proves the advantages and necessity of using the optimum similitude materials in scaled impact experiments.
- (5) For the similarity distortion of temperature softening effects, a technique of correcting adiabatic temperature rise is proposed in Section 3.3, which is further verified by the impact model of Taylor bar. Compared with the previous technique of correcting the initial temperature, the new proposed technique is more feasible since it not only is better applicable to the Johnson-Cook model but also can be conveniently applied to the actual impact experiment.

Since the material similarity is an important basic mechanical property of solid materials, it is necessary to be further explored in the future work of macroscopic and microscopic similarity of solids.

#### Authorship roles

Shuai Wang: Conceptualization, Methodology, Formal analysis, Writing – original draft; Fei Xu: Supervision, Methodology, Writing – review & editing, Resources, Funding acquisition; Xiaoyu Zhang: Investigation, Software; Leifeng Yang: Software, Validation; Xiaochuan Liu, Validation

#### Declaration of Competing Interest

The authors declare that they have no known competing financial interests or personal relationships that could have appeared to influence the work reported in this paper.

#### Acknowledgements

Preprint services of [preprints.org](https://www.preprints.org/manuscript/202011.0614/v1) for sharing our not peer-reviewed manuscript 24 November 2020 (<https://www.preprints.org/manuscript/202011.0614/v1>) is gratefully acknowledged.

This work is supported by the National Nature Science Foundations of China [grant no. 11972309] and the Overseas Expertise Introduction Project for Discipline Innovation (the 111 Project) [grant no. BP0719007].

#### Appendix A

The inaccuracy of the velocity correction factor Eq. (2) can be intuitively reflected by the similarity errors between the predicted stress  $(\sigma_d)_m / \beta_\sigma$  and the prototype stress  $(\sigma_d)_p$ . For example, the material strain hardening effects can be reflected by the simplified Johnson-Cook equation  $\sigma_d = A + B\varepsilon^n$ , where  $A, B$  and  $n$  are material parameters (see Appendix B). When the simplified equation is substituted into Eq. (2) with  $\varepsilon_p = 0.25$ ,  $\beta_V = 0.848$ , 0.697, 1.726, 2.126, 1.957, 1.230 and 0.908 can be obtained for the prototype with Nickel 200 and the scaled model respectively with other seven materials in Table B.1. Then, the stress prediction on the strain window  $[1E-4, 0.5]$  is shown in Fig. A.1. It can be seen that the predicted stresses of some materials (Cartridge Brass and OFHC copper) are close to that of the prototype, while others are very significantly different and even more than double that of the prototype, especially after using logarithmic coordinates perspective; and the perfectly accurate exists only if  $\varepsilon / \beta_\varepsilon = 0.25$ . The advantage of using logarithmic coordinates is that different orders of magnitude of strain can be adequately reflected. It is easy to verify that the same inexactness occurs for the material strain-rate sensitive and temperature softening effects.

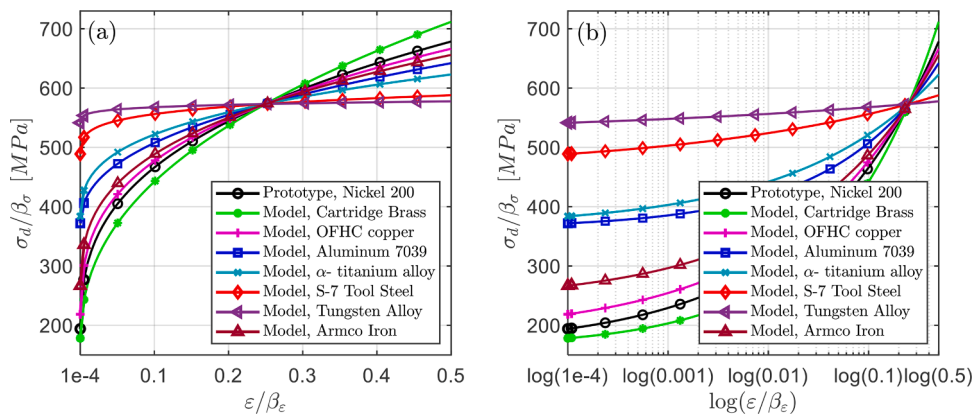


**Fig. A.1.** The significant similarity errors of the scaled model in predicting prototype stress indicate that the correction factor  $\beta_V$  (Eq. (2)) is not exact at scaling; (a) and (b), ordinary and logarithmic coordinates perspective for horizontal axis, respectively.

## Appendix B

The Johnson-Cook thermo-viscoplastic constitutive model [36] and material parameters used in this paper as follows.

The Johnson-Cook equation is expressed as

$$\sigma_d = (A + B\dot{\varepsilon}^n) \left( 1 + C \ln \left( \dot{\varepsilon} / \dot{\varepsilon}_0 \right) \right) (1 - T^{*m}), \quad (B.1)$$

where  $A$  is quasi-static flow stress;  $B$ ,  $n$ ,  $C$  and  $m$  are material constants;  $\dot{\varepsilon}^* = \dot{\varepsilon}/\dot{\varepsilon}_0$  with  $\dot{\varepsilon}_0$  being reference strain-rate;  $T^* = (T - T_r) / (T_m - T_r)$  with  $T_r$  and  $T_m$  being reference temperature and melting point, respectively.

Table B.1 Material properties of the Johnson–Cook constitutive equation.

Note: \* from [37]; \*\* from [38].

Material	Density [kg/m <sup>3</sup> ]	Elastic modulus [GPa]	Poisson's Ratio	T <sub>m</sub> [K]	Specific heat [J/kg·K]	A [MPa]	B [MPa]	n	C	̵̇ <sub>0</sub> [s <sup>-1</sup> ]	m
Cartridge Brass [36]	8.52E3	110 *	0.35*	1189	385	112	505	0.42	0.009	1	1.68
OFHC copper [36]	8.96E3	115 *	0.33*	1356	383	90	292	0.31	0.025	1	1.09
Nickel 200 [36]	8.90E3	204 *	0.31*	1725	446	163	648	0.33	0.006	1	1.44
Aluminum 7039 [36]	2.77E3	69 *	0.33 *	877	875	337	343	0.41	0.01	1	1.00
α-titanium alloy [39]	4.51E3 *	103 *	0.34*	1933**	470*	837	731	0.31	0.011	1	0.91
S-7 Tool Steel [36]	7.75E3	207 *	0.30*	1763	477	1539	477	0.18	0.012	1	1.00
Tungsten Alloy [36]	17.0E3	400 *	0.28*	1723	134	1506	177	0.12	0.016	1	1.00
Armco Iron [36]	7.89E3	207 *	0.30 *	1811	452	175	380	0.32	0.06	1	0.55

## References

- [1] Coutinho CP, Baptista AJ, Rodrigues JD. Reduced scale models based on similitude theory: a review up to 2015. Eng. Struct. 2016;119:81–94. <https://doi.org/10.1016/j.engstruct.2016.04.016>.
- [2] Casaburo A, Petrone P, Franco F, Rosa SD. A review of similitude methods for structural engineering. Appl. Mech. Rev. 2019;71(3):030802. <https://doi.org/10.1115/1.4043787>.
- [3] Jones N. Structural impact. Cambridge: Cambridge University Press; 1989.
- [4] Li G, Yu TX. Energy absorption of structures and materials. Cambridge: Cambridge Woodhead Publishing; 2003.
- [5] Zhao YP. Suggestion of a new dimensionless number for dynamic plastic response of beams and plates. Arch. Appl. Mech. 1998;68:524–38. <https://doi.org/10.1007/s0041990050184>.
- [6] Li QM, Jones N. On dimensionless number for dynamic plastic response of structural members. Arch. Appl. Mech. 2000;70:245–54. <https://doi.org/10.1007/s004199000072>.
- [7] Booth, E., Collier, D., Miles, J., 1983. Impact scalability of plated steel structures. In: Jones, N., Wierzbicki, T. (Eds.), Structural Crashworthiness, Butterworks, London, pp. 136–174.
- [8] Jones N, Jouri W, Birch R. On the scaling of ship collision damage, International Maritime Association of the East Mediterranean. Third Int. Congress Marine Technol. Athens 1984;2:287–94.
- [9] Wen HM, Jones N. Experimental investigation of the scaling laws for metal plates struck by large masses. Int. J. Impact Eng. 1993;13:485–505. [https://doi.org/10.1016/0734-743X\(93\)90120-V](https://doi.org/10.1016/0734-743X(93)90120-V).
- [10] Jiang P, Wang W, Zhang GJ. Size effects in the axial tearing of circular tubes during quasi-static and impact loadings. Int. J. Impact Eng. 2006;32:2048–65. <https://doi.org/10.1016/j.ijimpeng.2005.07.001>.
- [11] Fu S, Gao X, Chen X. The similarity law and its verification of cylindrical lattice shell model under internal explosion. Int. J. Impact Eng. 2018;122:38–49. <https://doi.org/10.1016/j.ijimpeng.2018.08.010>.
- [12] Hu YQ, Zhao YP. Scale effect of plastic strain rate. Chin. J. Aeronautics 2001;14: 37–43.
- [13] Drazevic P, Ravalard Y, Dacheux F, Marguet B. Applying non-direct similitude technique to the dynamic bending collapse of rectangular section tubes. Int. J. Impact Eng. 1994;15:797–814. [https://doi.org/10.1016/0734-743X\(94\)90066-T](https://doi.org/10.1016/0734-743X(94)90066-T).
- [14] Oshiro RE, Alves M. Scaling impacted structures. Arch. Appl. Mech. 2004;74: 130–45. <https://doi.org/10.1007/s00419-004-0343-8>.
- [15] Oshiro RE, Alves M. Scaling of cylindrical shells under axial impact. Int. J. Impact Eng. 2007;34:89–103. <https://doi.org/10.1016/j.ijimpeng.2006.02.003>.
- [16] Alves M, Oshiro RE. Scaling the impact of a mass on a structure. Int. J. Impact Eng. 2006;32:1158–73. <https://doi.org/10.1016/j.ijimpeng.2004.09.009>.
- [17] Jiang ZR, Zhong YK, Shi KR, Luo B. Gravity-based impact comparability rule of single-layer reticulated shells and its numerical verification. J. South China Univ. Techno. (Nat. Sci. Ed.) 2016;44:43–8. <https://doi.org/10.3969/j.issn.1000-565X.2016.10.007> (in Chinese).

- [18] Wei D, Hu C. Scaling of an impacted reticulated dome using partial similitude method. *Lat. Am. J. Solids Struct.* 2019;16:e158. <https://doi.org/10.1590/1679-78255342>.
- [19] Oshiro RE, Alves M. Scaling of structures subject to impact loads when using a power law constitutive equation. *Int. J. Solids Struct.* 2009;46:3412–21. <https://doi.org/10.1016/j.ijsolstr.2009.05.014>.
- [20] Alves M, Oshiro RE. Scaling impacted structures when the prototype and the model are made of different materials. *Int. J. Solids Struct.* 2006;43:2744–60. <https://doi.org/10.1016/j.ijsolstr.2005.03.003>.
- [21] Mazzariol LM, Alves M. Experimental study on scaling of circular tubes subjected to dynamic axial crushing using models of different materials. In: Proceedings of the 22nd international congress of mechanical engineering; 2013 (COBEM 2013).
- [22] Mazzariol LM, Oshiro RE, Alves M. A method to represent impacted structures using scaled models made of different materials. *Int. J. Impact Eng.* 2016;90: 81–94. <https://doi.org/10.1016/j.ijimpeng.2015.11.018>.
- [23] Mazzariol LM, Alves M. Similarity laws of structures under impact load: Geometric and material distortion. *Int. J. Mech. Sci.* 2019;157–8. <https://doi.org/10.1016/j.ijmecsci.2019.05.011>. 633–647.
- [24] Sadeghi H, Davey K, Darvizeh R, Darvizeh A. A scaled framework for strain rate sensitive structures subjected to high rate impact loading. *Int. J. Impact Eng.* 2019; 125:229–45. <https://doi.org/10.1016/j.ijimpeng.2018.11.008>.
- [25] Sadeghi H, Davey K, Darvizeh R, Darvizeh A. Scaled models for failure under impact loading. *Int. J. Impact Eng.* 2019;129:36–56. <https://doi.org/10.1016/j.ijimpeng.2019.02.010>.
- [26] Wang S, Xu F, Dai Z. Suggestion of the DLV dimensionless number system to represent the scaled behavior of structures under impact loads. *Arch. Appl. Mech.* 2020;90:707–19. <https://doi.org/10.1007/s00419-019-01635-9>.
- [27] Wang S, Xu F, Zhang X, Dai Z. Suggestion of a framework of similarity laws for geometric distorted structures subjected to impact loading. *Preprints* 2020; 2020020394. <https://doi.org/10.20944/preprints202002.0394.v1>. 2020.
- [28] Wang S, Xu F, Dai Z, et al. A direct scaling method for the distortion problems of structural impact. *Chin. J. Theoret. Appl. Mech.* 2020;52:774–86. <https://doi.org/10.6052/0459-1879-19-327> (in Chinese).
- [29] Davey K, Bilya O, Krishnamurthy B. Exact and inexact scaled models for hot forging. *Int. J. Solids Struct.* 2020;203:110–30. <https://doi.org/10.1016/j.ijsolstr.2020.06.024>.
- [30] Zhao YP, Liu S. On the definition of coefficient of strain-rate sensitivity. *Chin. J. Aeronautics* 2001;14:78–82. <http://www.hkxb.net.cn/cja/2001/01/0037/>.
- [31] Meyers MA, Chawla KK. Mechanical behavior of materials. New York: Cambridge University Press; 2009.
- [32] Bennett CJ. A comparison of material models for the numerical simulation of spike-forging of a CrMoV alloy steel. *Comp. Mater. Sci.* 2013;70:114–22. <https://doi.org/10.1016/j.commatsci.2013.01.003>.
- [33] Jones N. Dynamic inelastic response of strain rate sensitive ductile plates due to large impact, dynamic pressure and explosive loadings. *Int. J. Impact Eng.* 2014; 74:3–15. <https://doi.org/10.1016/j.ijimpeng.2013.05.003>.
- [34] Meyers, M. A., 1994. *Dynamical Behavior of Materials*. John Wiley & Sons.
- [35] Lu J, He YB, Tian CJ, Zhang FJ, Chen CJ, Deng HJ. Validation and optimization of dynamic constitutive model constants with Taylor test. *Explosion Shock Waves* 2006;26:339–44. <https://doi.org/10.3321/j.issn.1001-1455.2006.04.009> (in Chinese).
- [36] Johnson R, Cook WK. A constitutive model and data for metals subjected to large strains high strain rates and high temperatures. In: *The 7th International Symposium on Ballistics*. The Hague; 1983. p. 541–7.
- [37] William, D., Callister, Jr., 2007. *Materials science and engineering: an introduction*. John Wiley & Sons.
- [38] Khan AS, Suh YS, Kazmi R. Quasi-static and dynamic loading responses and constitutive modeling of titanium alloys. *Int. J. Plasticity* 2004;20:2233–48. <https://doi.org/10.1016/j.ijplas.2003.06.005>.
- [39] Bobbili R, Madhu V. Crystal plasticity modeling of a near alpha titanium alloy under dynamic compression. *J. Alloys Compounds* 2018;759:85–92. <https://doi.org/10.1016/j.jallcom.2018.05.167>.